ETH
Eidgenössische Technische Hochschule Zürich
Swiss Federal Institute of Technology Zurich

IAC Institute for Atmospheric and Climate Science

Master's Thesis

The stable water isotope structure of the July 2018 blocking event over the Eurasian Arctic

Department of Environmental Systems Science, ETH Zurich
Institute for Atmospheric and Climate Science

Supervisors

Franziska Aemisegger (main supervisor)
Institute for Atmospheric and Climate Science, ETH Zurich

Heini Wernli
Institute for Atmospheric and Climate Science, ETH Zurich

Submitted by

Janine Wetter
wetterj@ethz.ch
16-920-373

Zurich, April 8, 2021

Abstract

The Arctic is warming twice as fast as the global average, leading to a dramatic decrease in summer sea ice extent. Summers with a particularly strong sea ice reduction are characterized by enhanced anticyclonic circulation anomalies which further favour hot temperature extremes and forest fires in Scandinavia and the Russian Arctic. The strong surface-atmosphere coupling associated with relatively dry and cloud-free conditions plays a key role for the impact of such events on the environment. In this context an advanced understanding of the moisture structure of particularly persistent anticyclones (so called blockings) is important. In this regard, stable water vapour isotopes are a useful tool, as they are a natural tracer of the origin and moist processes experienced by air-parcels arriving in blocking anticyclones. In this Master's thesis, station-based stable water vapour measurements from Pallas (Finnland), satellite-based observations from the Tropospheric Monitoring Instrument (TROPOMI) and isotopic simulations from the isotope-enabled numerical weather model $COSMO_{iso}$ were combined with ERA5 reanalysis data to reconstruct the moisture sources of the particularly persistent blocking event in July 2018 with the help of backward trajectories. The isotope signature and humidity pattern associated with the anticyclone shows a spiral-shaped structure due to the clockwise circulation of the anticyclone with a more humid and enriched signal in the West and a drier and more depleted signal in the East. The total column integrated isotopic signal measured with the TROPOMI showed a slight shift of the spiral-shaped signature towards the South and fewer gradations between the very enriched (-120‰) and very depleted (-250‰) δD signals compared to the $COSMO_{iso}$ model simulations. A moist, high δD ring-like structure surrounding the anticyclone is found to be an artifact of the retrieval most likely related to scattering effects at the edge of cloudy regions. Furthermore, the Pallas ground-based observational isotope data showed that in the boundary layer also a spiral-shaped δD structure is visible. In the vertical a three layer structure was found in the anticyclone center with a moist and enriched surface layer followed by a dry layer above and another moist layer in the lower free troposphere. The moisture in the latter lower free tropospheric moist layer came from more southerly regions which are generally more humid and enriched in heavy isotopes than the moisture source regions of the drier layer. The moisture in the boundary layer was taken up locally by surface exchange. For future studies it would be interesting to compare this vertical three layer structure in the anticyclone center with other summer blocking events in the Eurasian Arctic.

Plain language summary

The Arctic warms more than the global average which leads to strong sea ice reduction during the summer months. High pressure systems that stay for several weeks over the Eurasian Arctic (so called blockings) are associated with summers of particularly strong sea ice reductions and further favour hot temperature extremes and forest fires in Scandinavia and the Russian Arctic. Previous studies explained this connection with fair-weather situations that are generally favoured by high pressure systems and therefore lead to enhanced warming radiation and reduced precipitation (due to reduced cloud cover) at the surface. Nevertheless, the importance of land-atmosphere coupling processes and feedbacks is not yet fully understood and therefore it is important to investigate the moisture structure and the related processes of such blocking events. For this purpose, water isotopes are a well-suited tool as they can tell us more about the moisture history of an air-parcel. Isotopes are water molecules with different masses. The more abundant light water molecules consist out of one oxygen atom and two hydrogen atoms while the heavy water molecules contain a deuterium instead of a hydrogen atom. Deuterium is a heavier version of the hydrogen atom because it contains one additional neutron in its core. In this Master's thesis different isotopic datasets were used to learn more about the moisture sources of such blocking events. Additionally, the pathways that air-parcels took during the last days before their arrival in the high pressure system (backward trajectories) were calculated with the help of special analysis tools and datasets that provided the necessary wind fields for the calculation. In this Master's thesis an especially strong blocking event in July 2018 was investigated. The moisture as well as the isotopic signal associated with the anticyclone, follow a spiral-like shape due to the general clockwise circulation of a high pressure system in the northern hemisphere. The western edge was more humid and enriched in heavy molecules while the air in the East was drier and more depleted in heavy water molecules. We observed a vertical three layer moisture structure in the center of the blocking. The layer close to the surface was moist and carried more heavy water molecules than the drier layer above. Above this drier layer an additional moist layer was found to frequently appear which is more enriched in heavy water molecules. These three layers differed in their origin. The air in the upper moist layer came from more southern regions that are generally warmer and more enriched in heavy water molecules than the air from the dry layer below that originated in the drier regions further north that carry less heavy water molecules. Moreover, the heavy isotopes close to the surface were taken up by evaporation of moisture at the Earth surface. For further studies it would be interesting to investigate if we see this vertical three layer structure in the moisture also for other summer blocking events in the Eurasian Arctic.

Contents

1 Introduction

In the last decades, the Arctic has warmed more than twice as fast as the global average - a phenomenon called Arctic amplification (Serreze et al., 2008; Screen and Simmonds, 2010; Cohen et al., 2014; Cowtan and Way, 2014). This has severe and very diverse consequences for the environment, such as glacial retreat (Dowdeswell et al., 1995; Overpeck et al., 1997), thawing permafrost (Lyon et al., 2009), changing habitats for local animals and ecosystems (Jay et al., 2012; Our Planet, 2019) and high rates of sea ice loss (Descamps et al., 2017). Anticyclones over the Arctic, north of Siberia, have been linked to enhanced Arctic summer sea ice loss and warm temperature extremes over the continental regions in summer (Pfahl and Wernli, 2012; Wernli and Papritz, 2018). The descending air in the center of these anticyclones favours fair-weather conditions (Ding et al., 2017) and thus increases the incoming short-wave radiation at the surface. This irradiation warms the surface (Trigo et al., 2004) and enhances summer sea ice melting in the European Arctic. In addition, it has also serious consequences for humans. These events can lead to dry fields and low river stages and enhance the risk of forest fires in Scandinavia and on the continental regions of Russia (Copernicus Climate Change Service (C3S), 2018). This has for example been shown for an anticyclonic event in July 2018, when a particularly persistent anticyclone dominated the northern Europe and Russian Arctic summer and lead to a strong heatwave. This summer was one of the hottest and driest in northern Europe (Watts, 2018; Sinclair et al., 2019).

While the radiative feedback of these anticyclones is well understood, not much is known about the moisture structure and transport that is responsible for the drought at the surface during these events. A better understanding of the moisture-related atmospheric processes in particularly persistent anticyclones (so called blockings) is thus needed to better protect the population from the consequences of such events.

This Master's thesis investigates the exceptional strong blocking event in July 2018 (00 UTC on 15 July 2018 until 23 UTC on 02 August 2018) in a case study and applies established analysis tools to study the moist processes associated with this summer blocking over the Eurasian Arctic. Backward trajectories help to understand the pathways of air-parcels before their arrival in the anticyclone and to explain the distribution of temperature, humidity and other properties in the blocking. Furthermore, stable water vapour isotopes are used to investigate the moisture origin and processes experienced by these air-parcels in the blocking. Stable water vapour isotopes are an especially useful tool to examine this, as they are a natural tracer of the origin and history of an air mass. The different physical properties of these isotopes (different saturation water vapour pressure and different diffusivities in air) lead to measurable physical changes, as the heavier isotopes preferably stay in the phase with stronger bonds (i.e liquid phase) in comparison to the lighter isotopes that more easily escape the phase with the stronger bonds (i.e. escape into the gaseous phase). In addition, another advantage is that they can be measured with ground-based or satellite-based instruments. A new type of such valuable observational data to investigate the isotopic signature of blocking events are shortwave infrared remote sensing retrievals from the Tropospheric Monitoring Instrument

(TROPOMI, Schneider et al. (2020)). This instrument is attached to a satellite and can measure the water vapour concentration and isotopic composition (δD signal) of the total atmospheric column by measuring the shortwave infrared radiation reflected by the Earth surface and the atmosphere and absorbed by HDO and $H_2{}^{16}O$ at different wavelengths (Veefkind et al., 2012). We will use the TROPOMI data in this Master's thesis to investigate the continental blocking event in July 2018. This data is only available for cloud-free regions over land for the published version of the retrieval. A new retrieval version, which takes into account scattering and allows retrievals over low clouds over land and ocean, is in development (Schneider et al., 2021).

Previous studies have shown that the center of this anticyclone over the European Arctic was generally dry and depleted in heavy isotopes while along the edge of the anticyclone a moister, cloudy ring-like structure of heavy isotopes can be observed (Schneider et al., 2020). This is assumed to be due to enhanced adiabatic descent in the center, which dries out the lower troposphere. As the descending air enters the boundary layer within the anticyclone, it is moistened due to surface fluxes, and due to the near-surface divergence it tends to transport this moisture away from the anticyclone center. To better understand the moisture and isotopic structure of this summer anticyclone over land, modelling data from the isotope-enabled regional numerical weather prediction and climate model $COSMO_{iso}$ are used in this Master's thesis. Additionally, ground-based humidity and isotope measurements from the Finnish weather station in Pallas should give an insight into the surface isotopic signal of the summertime blocking in 2018. The objective of this Master's thesis is to identify the physical processes that are responsible for the spatial variability with large horizontal gradients in the specific humidity and the heavy isotope composition within the summertime blocking in July 2018 and to help to improve the interpretation of satellite-retrieved stable water vapour isotope data.

This Master's thesis investigates the following research questions:

- What is the moisture structure of the summertime anticyclone in July 2018 over Scandinavia and the Russian Arctic?
- Where does the dry air in the center of the surface anticyclone in July 2018 originate? What is the vertical structure of the humidity and isotope signal in the core compared to the edge of the anticyclone?
- How do the simulated signals with the $COSMO_{iso}$ compare to the boundary layer observations and to the TROPOMI total column data?

In the following, a short general introduction into isotope physics (Section 2) and Arctic anticyclone dynamics (Section 3) is given. In Section 4 the datasets used for this Master's thesis are described, while the applied methods for the analysis can be found in Section 5. The results are presented and discussed in Section 6. Finally, a conclusion and an outlook are given in Section 7.

2 Theoretical aspects of isotope physics

Isotopes are atoms from the same element with a different amount of neutrons but an identical number of protons in their cores. For hydrogen (H) and oxygen (O) different stable isotopes exist and therefore, a water molecule (H_2O) can have different masses according to the isotopic composition of its hydrogen and oxygen atoms. In this Master's thesis we will focus on the hydrogen isotopes in stable, non-radioactive water molecules, so called isotopologues. Strictly speaking the term isotopes is only used to describe atoms (such as hydrogen atoms) with a different atomic mass while isotopologues is used for molecules (for example the water molecule H_2O) with the same molecular formula but a different molecular mass due to the different masses of their atoms (isotopes). To simplify the terminology in this thesis the term water isotopes is used instead of water isotopologues. The most abundant water isotopes are $^1H_2{}^{16}O$, $^1H_2{}^{18}O$, $^2H^1H^{16}O$ and $^1H_2{}^{17}O$. The ^2H atom is also called deuterium and often abbreviated as D. In Table 1 the natural abundance of the stable water isotopes is listed. This Master's thesis investigates the hydrogen isotopes ^1H and ^2H (deuterium). The oxygen isotopes are not taken into account in this thesis.

Isotope	**Relative Abundance [%]**	**Mass [u]**
$^1H_2{}^{16}O$	0.99731	18
$^1H_2{}^{18}O$	$2.000 * 10^{-3}$	20
$^1H_2{}^{17}O$	$3.789 * 10^{-4}$	19
$^2H^1H^{16}O$	$3.146 * 10^{-4}$	19

Table 1: Natural Abundance [%] and molecular mass in unified atomic mass unit [u] of the most abundant stable water isotopes listed according to their abundance (Gat (2010)).

The mass differences of the isotopes lead to measurable physical effects. The heavier isotopes prefer to stay in the phase with stronger bonds (i.e liquid) in comparison to the lighter isotopes that more easily escape from the liquid to the gaseous phase. This leads to preferential evaporation of the light isotopes during phase changes and consequently fractionation of the isotopes. The isotopic ratio R describes this difference in abundance of two isotopes in a given phase as a ratio between the concentration of the more rare isotope to the concentration of the more abundant isotope (which is i.e. the lighter molecule):

$$R = \frac{[\text{rare isotope}]}{[\text{more abundant isotope}]}$$

To compare different isotopic ratios, the R value of a water sample is compared with a reference isotopic ratio R_{Ref}. This difference is expressed with the delta (δ)

notation that is defined as follow:

$$\delta X = \frac{\mathrm{R(X)_{Sample}} - \mathrm{R(X)_{Ref}}}{\mathrm{R(X)_{Ref}}} * 1000(‰)$$

The δ value is given in permil (‰) and as R_{Ref} the mean isotopic ratio of ocean water is used. The usual R_{Ref} standard for δD (where $R_{Sample} = \frac{[\mathrm{DH^{16}O}]}{[\mathrm{H_2{}^{16}O}]}$) is the one of Vienna Standard Mean Ocean Water (VSMOW). The δ^2H value of ocean water is assumed to be approximately constant at a value of 0‰ and thus R_{Ref} is:

$R_{Ref}\,\mathrm{DH^{16}O} = 2{*}(155.76) \pm 0.1$ ppm

As explained above, phase changes of water lead to fractionation, but we need to distinguish between two different processes that lead to this fractionation:

Equilibrium fractionation
If the phase transition takes places during saturated conditions (relative humidity: 100%), the water molecules experience solely equilibrium fraction. The flux of molecules between the two phases is equal in both directions for each isotope. The fractionation between the light and heavy isotopes takes only place due to differences in the saturation water vapour pressure of the two isotopes (which is due to different binding energies and molecular structures of the isotopes) and is controlled by temperature. The lower the temperature the stronger the effect of fractionation.

Non-equilibrium fractionation
If the phase transition happens during non-saturated conditions (relative humidity not equal to 100%), an additional effect, the so called non-equilibrium fractionation effect, a secondary isotopic effect, comes into play. In this case a net water flux from one phase into another happens. As molecular diffusivities in air are higher for isotopically lighter molecules (i.e. H_2O) than for isotopically heavier molecules (HDO), more light isotopes will evaporate while the heavier molecules preferentially stay in the liquid phase. The air is therefore depleted in heavy isotopes compared to the liquid phase.

Isotopes have been widely used for paleoclimate reconstructions (Jouzel et al. (1982), Johnsen et al. (1989), Vimeux et al. (1999), Stenni et al. (2001), Masson-Delmotte et al. (2005), Steffensen et al. (2008)) and meteorological studies (e.g. Pfahl et al. (2012), Aemisegger et al. (2015), Aemisegger and Sjolte (2018)). In this Master's thesis we will use new observational isotope data from the TROPOMI satellite to learn more about the moist processes associated with the blocking event in the Eurasian Arctic in July 2018 and to better understand the isotopic structure of such an anticyclone.

3 Basic considerations on Arctic anticyclone dynamics

The differential warming of the tropics compared to the polar regions leads to a pronounced meridional temperature gradient. Due to the thermal wind relationship strong westward winds at upper levels form (mid-latitude jet stream). Such zones of baroclinic westerly flow are associated with strong wind shears and act as a waveguide along which Rossby waves can propagate (Hoskins et al. (1985), Martius et al. (2010)) and synoptic-scale cyclones and anticyclones, embedded in the so-called eddy-driven jet, can grow (Charney (1947), Eady (1949)). The storm track regions, which are the paths of travelling cyclones and anticyclones, are therefore closely linked to the location of the jet (Blackmon et al. (1977), Chang et al. (2002)). At upper levels, this band of anticyclones and cyclones that are embedded in the mid-latitude jet is visible as troughs and ridges.

At the eastern edge of an upper-level trough the air is ascending due to the tilted isentropes that ascend poleward. The surface cyclones that propagate along the eastern edge of the upper-level trough inject air masses with low potential vorticity (PV) into the Arctic upper troposphere. About half of the air masses experience substantial ascent and latent heating in a warm conveyor belt (WCB) and arrive as low-PV air in the upper troposphere (Madonna et al. (2014), Pfahl et al. (2015), Wernli and Papritz (2018)) . It is expected that the latent heating of the ascending air-parcels in the WCB plays an important role in the persistence of such blockings (Massacand et al. (2001), Grams et al. (2011)). The other half moved into the upper troposphere nearly along isentropic surfaces without latent heating (Pfahl et al., 2015). This advection of low PV air amplifies a ridge that is building in the upper troposphere along the mid-latitude jet and marks the onset of the blocking. During the subsequent days the upper-level ridge generally amplifies and results in an anomalously far poleward extension of the ridge and an intense upper-level anticyclonic flow anomaly (Steinfeld, 2019). The westerly polar jetstream is then blocked and guided northward around the ridge showing the reason why such persistent anticyclones are called blockings.

At the eastern edge of the ridge the air is descending along the isentropes and leads to a surface high pressure system. Therefore blockings often extend over the whole troposphere with a westward tilt with height. Due to the descending air, the core of the blocking anticyclone is mostly cloud-free which enhances the short-wave radiation at the surface and leads to warming (Steinfeld, 2019).

4 Data

To understand the humidity and isotope structure and related processes in the blocking system over Scandinavia and the Russian Arctic in July 2018, three different datasets were used: one reanalysis dataset (ERA5) and two isotope datasets (Pallas and TROPOMI). With the reanalysis dataset ERA5 we can investigate the distribution of different properties (e.g. temperature, relative and specific humidity, horizontal and vertical winds etc.) inside and around the anticyclone and on different pressure levels. The ERA5 data provides us the best available estimate of the large-scale meteorology. The two isotope datasets are observational data. The isotope dataset from the Finnish weather station in Pallas is measured at the ground. It helps to better understand the moisture and isotopic signature of the anticyclone at the surface and to investigate phase transition processes at the land-atmosphere interface when the descending dry air close to the center of the anticyclone reaches the surface. The second isotope dataset is the TROPOMI dataset. The instrument attached to the Sentinel-5 Precursor satellite provides a better understanding of the large-scale distribution of the isotopic signal inside and around the anticyclone. In this Master's thesis, these three datasets were combined with the model data from the isotope-enabled $\text{COSMO}_{\text{iso}}$ model (see Section 5.2) to compare different features from the modelled anticyclone with observations.

4.1 ERA5 - reanalysis data

The ERA5 reanalysis dataset (Copernicus Climate Change Service (C3S), 2017) from the European Centre for Medium Range Weather Forecasts was used on a horizontal grid of 0.5°x0.5° grid spacing and 137 vertical levels. For the analysis, hourly data was used. To characterise the features of the anticyclone event in July 2018, different properties were investigated with the ERA5 data: temperature, relative and specific humidity, pressure, total cloud cover, total column water (TCW), horizontal and vertical winds, PV at upper tropospheric levels (on 325 hPa), geopotential height, potential temperature, T2m, evaporation and precipitation. The ERA5 reanalysis dataset enabled us to investigate the large-scale synoptic situation and to perform an Eulerian analysis of the spatial distribution of different thermodynamic variables inside the anticyclone throughout the anticyclone lifetime (see Section 6.2.1). This analysis provided the basis for the meteorological understanding of the anticyclone's temporal evolution and is combined later on with a Lagrangian analysis that was conducted with the ERA5 data and the $\text{COSMO}_{\text{iso}}$ model (see Section 6.2.2). In this context, the ERA5 data was used to validate the results from the $\text{COSMO}_{\text{iso}}$ model simulations (see Section 5.2) as the ERA5 reanalysis data provides the best possible representation of the large-scale situation.

The ERA5 dataset replaced the ERA-Interim reanalysis data (Hoffmann et al., 2019). Hoffmann et al. (2019) found differences in specific humidity along the backward trajectories after one day of up to 30% between the two datasets. These differences are due to the improved spatial resolution in ERA5, changes in the forecast model, in available observations and in the data assimilation system (Hoffmann

et al., 2019). In this Master's thesis, the main reason for using the ERA5 reanalysis data is the hourly resolution (compared to ERA-Interim that is only available 6-hourly) and the increased spatial resolution. This provides a more detailed insight into the evolution of the anticyclone's moisture structure throughout the course of a day in particular at lower-levels.

4.2 Pallas - ground-based isotope data

Hourly water vapour data (atmospheric water vapour concentration and stable water vapour isotope (δD) signal) from the Finnish weather station Pallas (Sammaltunturi Station, Pallas-Yllastunturi National Park operated by the Finnish Meteorological Institute, 67.97°N 24.12°E, 555 m a. s.l., see Figure 1) was used. The data covers the anticyclonic event in July 2018 (00 UTC on 15 July 2018 until 23 UTC on 02 August 2018). It was recorded with a cavity ring-down laser spectrometer from Picarro and provided by Hannah Bailey and Jeffrey Welker from the University of Oulu, Finland. The measurement accuracy is estimated at ± 0.6‰ for δD following all standard and humidity concentration corrections. The measurement precision estimated from the standard deviation of the calibration measurements at a constant humidity level is ± 0.8 for δD at humidity levels >2 g kg^{-1}.

4.3 TROPOMI - remote sensing total column data

The TROPOMI instrument onboard the Sentinel-5 Precursor satellite provides a new dataset of concentrations of the stable water vapour isotopes H_2O and HDO, integrated over the whole atmospheric column. As the two isotopes absorb reflected short-wave infrared radiation from the surface at two slightly different wavelengths at around 2.3 μm, we can differentiate between the two isotopes and deduce accordingly their total column densities. The TROPOMI data features daily global coverage, while the satellite is orbiting the Earth, with a spatial resolution of up to 7 km x 7 km in the center of the 2600 km swath (Veefkind et al., 2012) since 9 November 2017 until present. For this Master's thesis, only data over the Eurasian Arctic was used that further covered the Finnish weather station in Pallas. TROPOMI provides no data over oceans because ocean water does not reflect enough radiation in the short-wave infrared range. Furthermore, the data is filtered for cloud-free regions because scattering from clouds is not taken into account in the retrieval algorithm used and would imply wrong stable water isotope column densities. A new retrieval version, which takes into account scattering and allows retrievals over low clouds over land and ocean is in development (Schneider et al., 2021).

The non-scattering TROPOMI dataset is provided by Andreas Schneider and Tobias Borsdorff from Neatherlands Institute for Space Research. The accuracy is higher in the low and mid-latitudes than in the high latitudes where the solar zenith angles are larger and therefore the light pathways longer. Moreover, the albedo is lower in the high latitude land regions in summer (Schneider et al., 2020). The uncertainties are, however, smaller than the amplitude of the spatial variability observed in Arctic blocking anticyclones (Schneider et al., 2020), making the TROPOMI data suitable

for the investigation of high latitude anticyclones in this Master's thesis. Due to the fact that the TROPOMI measures short-wave infrared instead of thermal infrared as many other instruments do (such as IMG, TES, MIPAS, IASI and AIRS, which have their largest sensitivity in the stratosphere and upper troposphere), the TROPOMI is very sensitive in the lower troposphere, including the boundary layer close to the surface. TROPOMI uses the same spectral range as the older shortwave infrared instrument SCIAMACHY but has a better signal-to-noise ratio and an unprecedented spatial resolution. As we expect that a large part of the humidity is located in the lower troposphere, the latter sensitivity feature from the TROPOMI instrument is very helpful for this Master's thesis.

5 Methods

This Master's thesis applied established modelling tools and Lagrangian diagnostics that have never been used before to analyze the moisture structure of summer Eurasian Arctic blockings. These methods are described in more detail in the following. First, the anticyclone mask, an algorithm to detect anticyclones, is described. Afterward, the isotope-enabled numerical weather model $COSMO_{iso}$ and its set-up is explained, followed by a detailed explanation of the set-up of the backward trajectories for ERA5 and $COSMO_{iso}$. Finally, the calculation of the moisture sources is described.

5.1 Anticyclone mask

To detect the anticyclone during the July 2018 event, an algorithm developed by Wernli and Schwierz (2006) and slightly adapted by Sprenger et al. (2017) was used. This algorithm can be applied to the ERA5 sea level pressure data and was originally developed to detect cyclones. For this Master's thesis the algorithm was modified and adapted by Michael Sprenger from the Institute for Atmospheric and Climate Science at ETH Zurich to be able to detect anticyclones. The algorithm identifies the anticyclone center as a local maximum in the sea level pressure field. The area of the anticyclone is then defined as the outermost closed sea level pressure contour enclosing the sea level pressure maximum. The anticyclone was tracked in this Master's thesis with hourly ERA5 data. More details about this methodology can be found in Wernli and Schwierz (2006) and Sprenger et al. (2017).

5.2 $COSMO_{iso}$ - Isotope enabled numerical weather prediction model

The limited-area regional numerical weather prediction model COSMO (Consortium for Small-scale Modeling, Steppeler et al. (2003)) is used in its isotope-enabled version $COSMO_{iso}$ (Pfahl et al., 2012) with two additional parallel water cycles for the heavy water isotopes $H_2{}^{18}O$ and ${}^{1}H^{2}H^{16}O$, which mirror the water cycle of the light, most abundant water isotope $H_2{}^{16}O$. These two additional water cycles are affected by the same physical processes except that they experience isotopic fractionation during phase change processes. The model $COSMO_{iso}$ has been previously used in other studies to investigate various aspects of the regional atmospheric water cycle over Europe and the USA (e.g. Pfahl et al. (2012), Aemisegger et al. (2015), Christner et al. (2018), Dütsch et al. (2018), Lee et al. (2019)). In this Master's thesis, a $COSMO_{iso}$ simulation is conducted, covering the Eurasian Arctic (see Figure 1) during the blocking event in July 2018.

The simulation was initialised by data of the global isotope-enabled model ECHAM5-wiso, provided by Martin Werner from the German Alfred-Wegener-Institute. The same data was used at the lateral boundaries of the $COSMO_{iso}$ domain. The $COSMO_{iso}$ simulation was spectrally nudged to the winds above 850 hPa of the ECHAM5-wiso data to make sure that the meteorology in the regional $COSMO_{iso}$

Figure 1: The $COSMO_{iso}$ domain that was used in this Master's thesis (green line) and the location of the Finnish weather station in Pallas (red cross) at 24.12° N and 67.97° E.

model does not deviate too much from the global model. The ECHAM5-wiso simulation itself was nudged (surface pressure, temperature, divergence and vorticity) to the ERA-Interim reanalysis data (Werner et al. (2011), Butzin et al. (2014)). The ECHAM5-wiso fields are available 6-hourly with a spectral resolution of T106 (corresponding to 88 km at 45°S) and 31 vertical levels (Thurnherr et al., 2020a). The $COSMO_{iso}$ simulations were performed at a horizontal resolution of 0.2°, corresponding to ∼20 km, with 40 vertical levels and explicit convection. The explicit convection setup is preferred over using the deep convection parametrisation even at the relatively coarse resolution used here (Thurnherr et al., 2020a). Vergara-Temprado et al. (2020) have shown that simulations with the COSMO model over Europe represent the hydroclimate more realistic in this setup. Furthermore, simulations with the isotope-enabled version $COSMO_{iso}$ over the Southern Ocean with explicit convection revealed a reduced strength of vertical mixing and the vertical isotope profiles were more realistic than with parametrised convection (Jansing, 2019).

The isotopic fractionation during surface evaporation is parametrized with the Craig-Gordon model (Craig and Gordon, 1965) using a wind speed independent formulation of the non-equilibrium fractionation factor corresponding to the Merlivat and Jouzel fractionation factor at 6 ms^{-1}. The isotopic composition of the ocean surface water is prescribed at a constant value of 1‰ for δ^2H and $\delta^{18}O$. For more details about the physics and the isotope parametrisation in the $COSMO_{iso}$ model see Doms et al. (2011) and Pfahl et al. (2012). For terrestrial surfaces, a one-layer surface snow model with equilibrium fractionation during snow sublimation (phase transition from solid snow to gaseous water vapour) and a multi-layer soil model (see supplement of Christner et al. (2018)) was used. For this analysis hourly $COSMO_{iso}$ simulation outputs were used and the $COSMO_{iso}$ domain is shown in Figure 1.

Calculation of Total Column δD (δD_{tot})
In this Master's thesis, the $COSMO_{iso}$ isotope signal was compared with the satellite-based observational isotope data from the TROPOMI. As the TROPOMI signal is a vertical column integrated isotope signal, the $COSMO_{iso}$ isotope signal was integrated over the whole vertical atmospheric column. The $COSMO_{iso}$ total column δD (δD_{tot}) was calculated as follow:

$$\delta D_{\text{tot}} = \left(\frac{R_{\text{tot}}}{R_{\text{VSMOW}}} - 1 \right) * 1000$$

where R_{VSMOW} is the mean isotopic ration of ocean water according to the VSMOW standard (see Section 2) and

$$R_{\text{tot}} = \frac{\int_{p_{\text{surf}}}^{p_{\text{top}}} [HDO] dp}{\int_{p_{\text{surf}}}^{p_{\text{top}}} [H_2O] dp}$$

5.3 Backward trajectories

Ten-day (eight-day) backward air-parcel trajectories were calculated based on the three-dimensional wind fields from ERA5 ($COSMO_{iso}$) with the Lagrangian Analysis Tool LAGRANTO (Wernli and Davies (1997), Sprenger and Wernli (2015)) for the July 2018 event (00 UTC on 15 July 2018 until 23 UTC on 02 August 2018). The $COSMO_{iso}$ backward trajectories were only calculated eight days back in time as most of them have already left the $COSMO_{iso}$ domain defined for this Master's thesis (see Figure 1) at this point and they were used in addition to the ERA5 backward trajectories because the ERA5 data can not show the isotopic signal. The backward trajectories help us to understand the temporal evolution of different properties (i.e. temperature, relative and specific humidity etc.) inside and around the anticyclone. For this different 3D and 2D variables were interpolated to the trajectory's position, including pressure, specific humidity and the δD signal (for the $COSMO_{iso}$ trajectories). Trajectories for the anticyclone center region were calculated with the ERA5 data and the $COSMO_{iso}$ model to compare the two outputs. For the ERA5 ($COSMO_{iso}$ model) 100 trajectories were started inside a radius of 500 km around the anticyclone core between 700-1000 hPa (500-1000 hPa) on 10 (50) vertical layers. The center was determined as the location with the highest sea level pressure. Sometimes, when for example two locations inside the anticyclone mask showed the same sea level pressure or the anticyclone merged with a second anticyclone, the anticyclone center was determined manually. Please note that the center for the ERA5 data and the $COSMO_{iso}$ model vary due to the different datasets they use. On average the longitude (latitude) of the anticyclone core in the ERA5 data is 0.222° (0.079°) larger than the longitude (longitude) from $COSMO_{iso}$ but this is not a significant difference (t-test p=0.815 respectively p=0.792). With the $COSMO_{iso}$ model additional trajectories were calculated for the regions east and west of the center. Therefore, again 100 trajectories between 500-1000 hPa on 50 vertical levels were calculated that lie within a circle of 500 km radius that was shifted 25 km to the East and to the West from the core.

Anticyclone-centered trajectories
To get an overview of the different backward trajectories arriving in the center at different times during the event, averaged anticyclone-centered trajectories were calculated. Anticyclone-centered means that we calculated the trajectories relative to the anticyclone core, independent of the latitude and longitude at which the anticyclone core was situated. Therefore, for every day of the event every trajectory arriving in a specific vertical layer (in total three different vertical layers were investigated) was averaged with the other trajectories fulfilling this conditions. Afterward, we had 19 averaged trajectories (one for each day of the event). Finally, the trajectories were colored with the corresponding averaged pressure or isotopic or specific humidity signal.

5.4 Moisture source diagnostics

The moisture sources of the air-parcels arriving in the center and the eastern and western anticyclone region are analyzed using the method of Sodemann et al. (2008). This method is particularly useful as it provides us a quantitative estimate of the moisture uptake regions of the humidity arriving in the anticyclone. The moisture sources were calculated based on the trajectories computed from ERA5 and the $\text{COSMO}_{\text{iso}}$ simulation, as described in Section 5.3.

In short, this method considers the mass budget of water vapour in an air-parcel. Whenever the specific humidity of an air-parcel along its trajectory increases, this is registered as a moisture uptake. The weight of each uptake determines the relative contribution to the final humidity of the air-parcel at its arrival. Decreases in specific humidity indicate precipitation and are registered as a humidity loss. In this case, the weight of all previous uptakes is reduced proportionally to the loss of humidity during the precipitation event. In the end, the identified moisture sources of a trajectory are weighted by the air-parcel's specific humidity at arrival to get the relative contribution of each uptake to the final humidity (Sodemann et al., 2008; Aemisegger et al., 2020). This method has already been used in other studies, mainly for the interpretation of water isotope signals in vapour and precipitation (e.g. Pfahl and Wernli (2008), Aemisegger et al. (2014), Aemisegger (2018), Aemisegger et al. (2020), Thurnherr et al. (2020b)).

In this Master's thesis the moisture sources were not analyzed for single trajectories but for trajectory bundles, where multiple trajectories were put together to analyze the moisture source of these so called airstreams. The advantage of this procedure is that we can analyze the moisture source of a certain subregion in the anticyclone by selecting the trajectories arriving in a specific region. The trajectories chosen for this analysis are the same as defined in Section 5.3 for the three subregions in the center, the East and the West. The center was analyzed with ERA5 and $\text{COSMO}_{\text{iso}}$ trajectories while for the eastern and western region only trajectories with the $\text{COSMO}_{\text{iso}}$ were calculated and used for the moisture source diagnostics (MSD). For each of these three subregions the trajectories were further divided into three vertical layers. This was done due to the vertical moisture structure of the anticyclone, as described later in Section 6.2. For the ERA5 data, the levels were

900-1000 hPa, 800-900 hPa, 700-800 hPa. For the $COSMO_{iso}$ model the vertical layers were 900-1000 hPa, 750-850 hPa and 500-700 hPa. Different vertical levels were chosen for the ERA5 and the $COSMO_{iso}$ because their moisture structure was vertically shifted as they are based on different datasets. In this Master's thesis, the layer close to the surface was named "boundary layer" (BL), the layer on top "dry layer" (DL) and the uppermost layer "moist blob" (MB).

6 Results and discussion

To better understand the moisture structure and processes associated with the Eurasian Arctic anticyclone at the end of July 2018, we first describe the synoptic situation, in which it was embedded to get a better understanding of the large-scale environment (Section 6.1). Second, one specific timestep during the event was chosen, namely 23 UTC on 28 July 2018, to investigate the moisture structure, the circulation and the associated isotopic distribution in detail (Section 6.2). Finally, the study was expanded to the whole July 2018 event (Section 6.3).

6.1 Large-scale synoptic situation during the July 2018 event

In the following, four timesteps during the blocking anticyclone event in July 2018 (from 00 UTC on 15 July 2018 until 23 UTC on 02 August 2018) over Scandinavia and the Russian Arctic were chosen to describe the synoptic evolution of this persistent event (see Figure 2). The plots are based on the ERA5 reanalysis data.

On 15 July 2018 the anticyclone formed over the North Sea, North-Germany and Denmark and expanded further towards Norway. During the following days (16 to 18 July 2018) the anticyclone expanded northward and stayed relatively stationary with its center located over Northeast Russia and the White Sea. On 19 July 2018 the anticyclone then moved eastward and a small high pressure system that originated in the North Sea merged from the West. A band of humid air could be observed between the two merging anticyclones. The next day, the anticyclone expanded further in a zonal direction and moved eastward over Northern Russia and the Kara Sea.

At 11 UTC on 21 July 2018 the anticyclone reached its largest zonal expansion by spreading over 140-longitudinal degrees (see anticyclone mask in Figure 2a,b,c). The horizontal winds on 900 hPa blew in a clockwise direction around the anticyclonic center and showed some divergence away from the center (violet arrows in Figure 2a). This divergence can occur due to the descending air in the center that diverges close to the surface. In the temperature signal on 900 hPa in Figure 2a we see that the regions more poleward are generally colder than the regions further south. In the vicinity of the anticyclone the temperature was twisted like a spiral around the anticyclone center due to the northward (southward) blowing wind at the western (eastern) edge of the anticyclone that transported warm (cold) air from the South (North) towards the North (South). The same spiral-shaped structure can be seen in Figure 2b for the TCW for the same reason and because the more southerly (northerly) regions are generally more humid (drier) than the regions further north (south).

Another typical feature of the anticyclone is visible in Figure 2b which shows an almost cloud-free center with a cloudy, ring-like structure surrounding it. During its descent the air in the center warms due to adiabatic compression which increases its water carrying capacity and decreases its relative humidity. This leads to the dissipation of clouds, that normally form at the boundary layer top under saturated

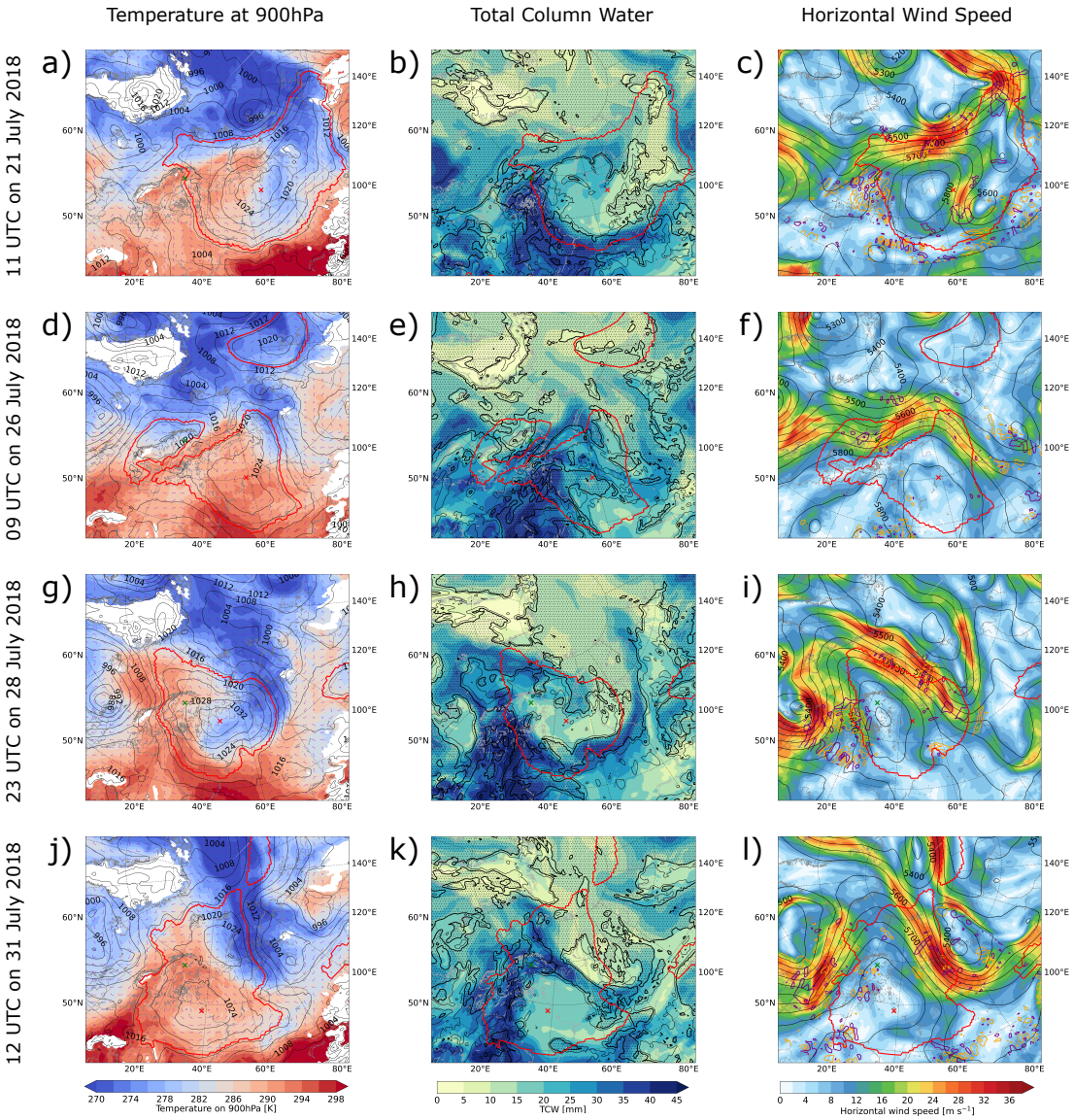

Figure 2: The red contour in all pictures shows the anticyclone mask, the red cross shows the anticyclone center and the green cross the location of the Finnish weather station in Pallas. In the left column the temperature at 900 hPa is shown with the sea level pressure contours in black and the horizontal wind at 900 hPa with violet arrows, based on the ERA5 reanalysis data. The middle column shows the total column water (TCW) with the total cloud cover shown as black contours (thin black line = 30% cloud cover, thick black line = 80% cloud cover, dotted area = more than 80% cloud cover). The right column shows the horizontal wind on 500 hPa, the geopotential height of the 500 hPa pressure surface as black contours and the vertical wind on 500 hPa as colored contours (orange = downward wind, violet = upward wind). The anticyclone (indicated by the red anticyclone mask) with a red cross in the center is the anticyclone we are investigating in this Master's thesis.

conditions. Finally, Figure 2c shows us that the westerly polar jetstream that normally circulates between 40°-60°N was shifted northward to about 75°N due to the blocking anticyclone.

At the end of 21 July 2018 the anticyclone shrunk strongly before it started to expand towards the North and built a second maximum in sea level pressure the next day. The northerly high pressure center intensified during its evolution and started to move eastward on 23 July 2018. In the morning of 24 July 2018 the two high pressure centers then split and the southerly anticyclone stayed stationary for the rest of the day with its center over Northwestern Russia, south of the Barents Sea. Due to the splitting more humid air was advected around the northern tip of the southerly anticyclone (not shown).

In the morning of 25 July 2018 the pressure of the anticyclone core increased by about 4 hPa in only a few hours due to an intrusion of anticyclonically recurving moist air from the Southwest into the center. This lead to cloud formation in the otherwise almost cloud-free anticyclone core (Figure 2e). At 10 UTC on 26 July 2018 another anticyclone that formed over the North Sea merged with the larger anticyclone. Figure 2e shows that a band of humid air was advected in between the two anticyclones.

After the merging, the northwestern high pressure center strongly increased in pressure during the course of the 26 and 27 July 2018 until it reached a pressure of more than 1032 hPa, which is higher than the pressure in the original anticyclone core in the Southeast. Finally, the previous pressure center weakened and cutted-off in the Southeast.

At 23 UTC on 28 July 2018 the anticyclone was enclosed by two cyclones, one to the West and one to the East, and another anticyclone in the Southwest (Figure 2g). This configuration amplified the ridge and the horizontal winds on 500 hPa (Figure 2i).

On 29 and 30 July 2018 the anticyclone expanded over the Greenlandic ice sheet and moved towards the East where it formed a second high pressure center. These two, still connected high pressure centers, shrunk during the course of the 30 July 2018 and were separated by a band of humid air (Figure 2k). Finally, at 12 UTC on 31 July 2018, the anticyclone reached its maximum meridional extension, covering almost 40-meridional degrees (see Figure 2j,k,l).

Towards the end of the event, the anticyclone shrunk strongly and fast and with the southward movement of the northernmost point of the anticyclone, the jet stream finally also moved south again. On 01 August 2018 the two anticyclone centers finally spilt, moved further south and shrunk. The more easterly center disappeared while the anticyclone more to the West merged with another larger anticyclone in the West and disappeared completely together with this anticyclone at the end of 02 August 2018. With the disappearing of the anticyclone also the spiral-shaped structure in the temperature and TCW dispersed and formed a North-South distribution again, with cold and dry air in the North and warm and more humid air in the South.

6.2 Detailed analysis of the humidity and isotope structure of the established anticyclone (23 UTC on 28 July 2018) and links to the dynamics

6.2.1 Eulerian characteristics

In this Section we look at one specific timestep during the July 2018 event, namely 23 UTC on 28 July 2018, to better understand the key features of this anticyclonic event. This timestep was chosen because the anticyclone was very circular and constant in size and its center stayed over the same location for several hours.

In the following, an Eulerian analysis was conducted for 23 UTC on 28 July 2018 where the distribution of different properties in the anticyclone is described. In Section 6.2.2 we will then investigate the airstreams and the associated transport processes that lead to the patterns we identified in the Eulerian analysis in this Section.

Figure 3 shows the temperature (left column) and the specific humidity (right column) distribution at different pressure levels (950 hPa, 850 hPa, 750 hPa). For the temperature we see at all pressure levels that the region in the Southwest is generally warmer by about 20K than the region in the Northeast. The temperature distribution follows a spiral-shaped signature that is twisting around the center in a clockwise direction and the temperature generally decreases with increasing altitude.

The specific humidity also shows a spiral-like signature on all pressure levels (right column of Figure 3) with more humid air in the Southwest and air that is about 6 g kg^{-1} drier in the Northeast. Along the edge of the anticyclone, the specific humidity generally decreases with height while, surprisingly, we see a different trend in the center. From 950 hPa to 850 hPa the center gets drier with increasing altitude, while the specific humidity increases again towards 750 hPa.

To investigate the moisture structure and especially this locally increased specific humidity in the lower free troposphere in the core of the anticyclone in more detail, zonal (from East to West) and meridional (from North to South) vertical cross sections through the center were made. Figure 4 shows the location of the zonal (black) and meridional (blue) cross sections that were made for 23 UTC on 28 July 2018.

In Figure 5a we see that the eastern and western edge generally contain more humidity than the anticyclone center. Close to the surface the humidity is especially high in the western edge region which is influenced by the advected air from the humid regions in the South. Above 900 hPa the edges contain clearly more humidity than the center on the same pressure level but we also see that the air in the East and West that is located near the center is still very dry above 800 hPa, indicating that this air is still influenced by the descending air in the center.

We can see similar features in the meridional cross section in Figure 5b where the specific humidity is higher along the anticyclone edges in the North and South than

in the center. Further, we see that the southern edge is associated with very high values of specific humidity close to the surface compared to the center and the northern edge because locations further south generally contain more moisture.

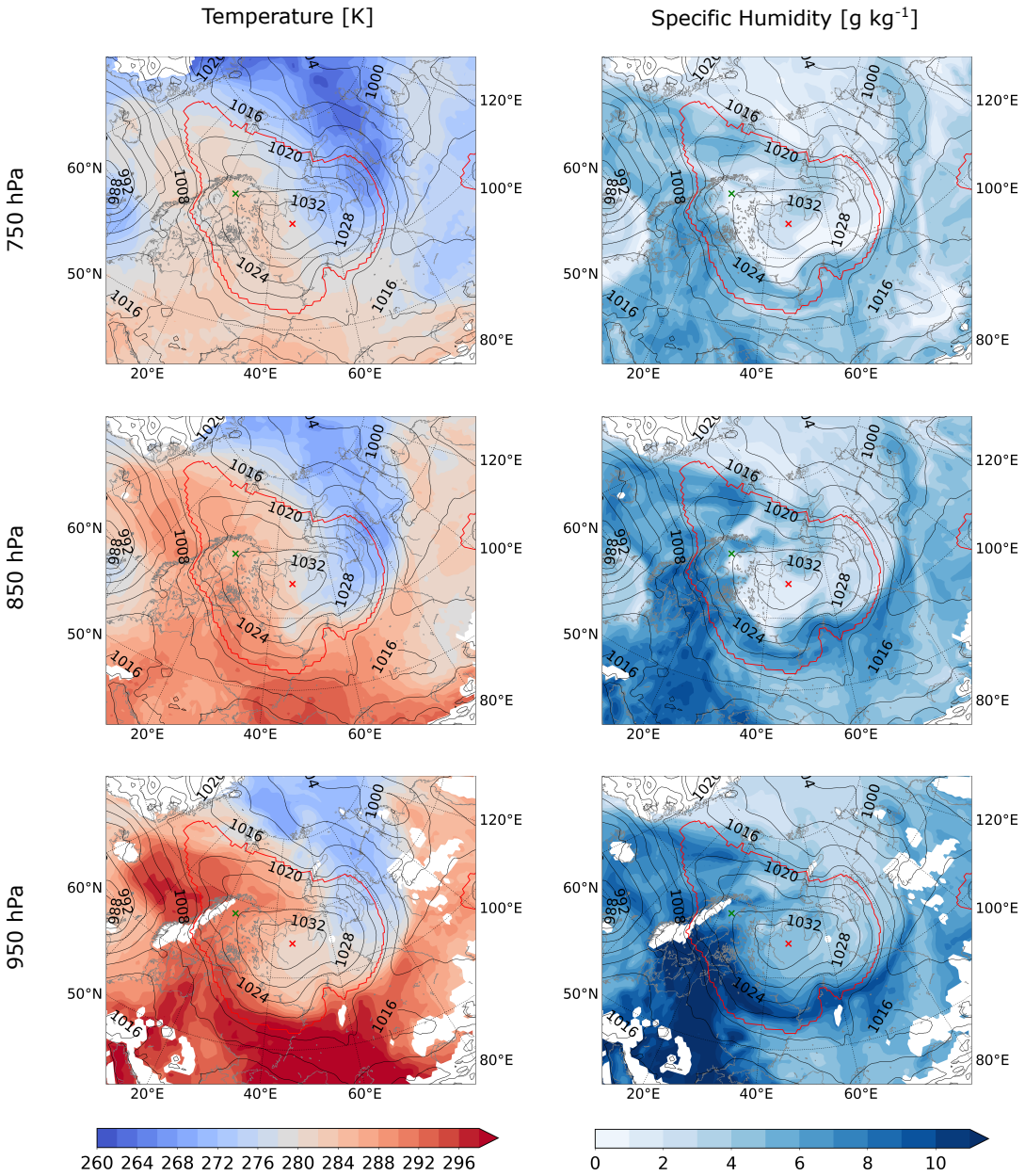

Figure 3: The red contour in all pictures shows the anticyclone mask, the red cross shows the anticyclone center and the green cross the location of the Finnish weather station in Pallas. In the left column the temperature at the indicated pressure levels (950 hPa, 850 hPa and 750 hPa) is shown. In the right column the specific humidity at the same pressure levels is presented. The plots are based on the ERA5 reanalysis data.

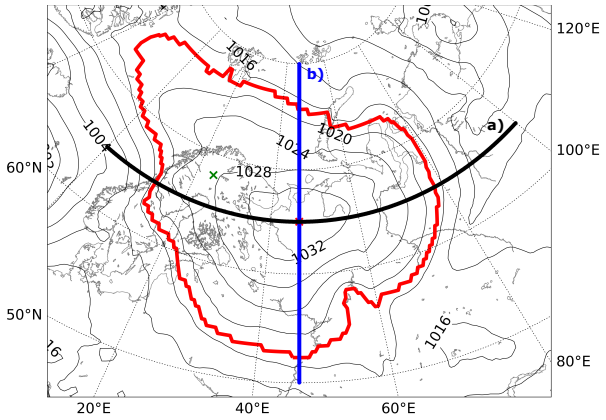

Figure 4: Zonal (a, black) and meridional (b, blue) vertical cross section through the anticyclone center at 23 UTC on 28 July 2018 as shown in Figure 5a,b.

In the anticyclone center in Figure 5a and b we see the special humidity structure again that we have already observed in Figure 3. The air close to the surface (900-1000 hPa) carries more humidity than the air higher up between approximately 800-900 hPa. Surprisingly, the humidity then increases again in both cross sections when we go to a pressure level between 600-800 hPa. In this Master's thesis the moist layer close to the surface in the center is called "boundary layer" (BL), the dry layer on top of the BL is called "dry layer" (DL) and the uppermost moist layer is named "moist blob" (MB), as illustrated in Figure 5. In the following we will use backward trajectories to better understand the circulation and dynamics that lead to this vertical moisture layering.

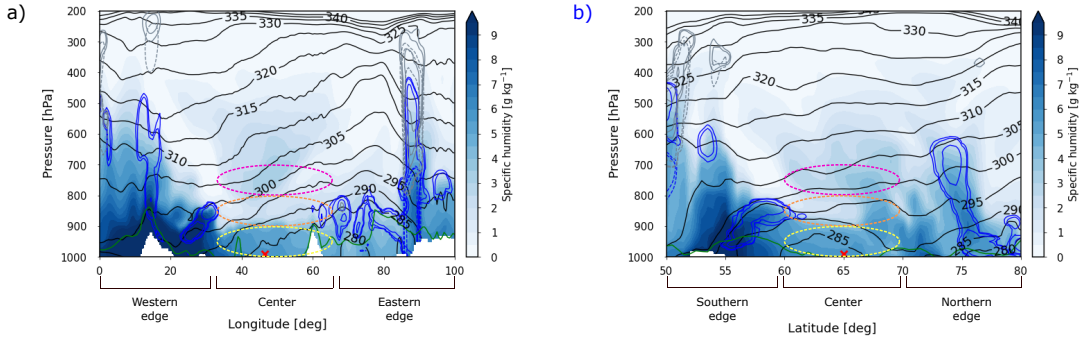

Figure 5: Vertical cross sections through the anticyclone center in a) zonal and b) meridional direction. The specific humidity is indicated in blue colors and the anticyclone center is indicated by the red cross. The black contours show the potential temperature, the blue (liquid water, rain) and grey (ice and snow) contours show liquid-water and ice clouds (solid line) and snow- or rainfall (dashed lines). The green line indicates the boundary layer height. The pink circle indicates the MB, the orange circle the DL and the yellow circle the BL. Along the x-axis the regions are labeled.

6.2.2 Transport and moisture sources

To understand why we observe the humidity distribution we just described in the previous Section it is important to better understand the circulation in and around the anticyclone. Therefore, a Lagrangian study was conducted. Backward trajectories were calculated with the ERA5 data and the $COSMO_{iso}$ model for the three vertical layers BL, DL and MB in the anticyclone center. The ERA5 trajectories were colored with the pressure while the $COSMO_{iso}$ trajectories were colored with the δD signal. The $COSMO_{iso}$ trajectories showed a very similar pressure signal along the trajectories as the ERA5 data (not shown). For this reason we can assume that the $COSMO_{iso}$ trajectories behave similar as the ERA5 trajectories in ascent and descent (Figure 6, left column) and that the ERA5 trajectories can be used later (Section 6.2.3) in combination with the analysis of the isotopic signal along the trajectories (Figure 6, right column). Additional backward trajectories were calculated with the $COSMO_{iso}$ model for the eastern and the western edge regions on the same three vertical levels as for the center. Please note that the vertical levels in the ERA5 data and the $COSMO_{iso}$ model were shifted due to the slightly different flow conditions in the two datasets (see Section 5.4). In this Section we will first investigate the trajectories that arrived in the center and later also the ones that arrived in the eastern and western edge regions.

Center backward trajectories

A general feature we can observe in Figure 6 on all pressure levels is that almost all trajectories in the center came from the West and entered the anticyclone in the North, while recurving clockwise towards the center. The air then descended strongly when it came closer to the core, especially in the BL and DL (Figure 6c,e). Generally, the ERA5 and the $COSMO_{iso}$ show similar trajectories for the different layers in the center.

The trajectories in the BL can be roughly grouped into three bunches of air-parcels, so-called airstreams (Figure 6e,f). The first airstream came from Canada from about 55°N and ascended by about 150 hPa while it moved along the Norwegian coast. Another airstream originated from a few degrees further north (about 60°N) and descended by about 150 hPa on its way to the North of Norway. The third, a much smaller airstream, came from about 75-80°N and moved, according to the ERA5 data (Figure 6e), around half of the globe close to the North Pole on a low pressure level (500-600 hPa). The $COSMO_{iso}$ trajectories show a similar feature (Figure 6f) but we can not observe this advection around the pole due to the limited $COSMO_{iso}$ domain. The $COSMO_{iso}$ backward trajectories show that another small airstream originated from the East. I expect that these air-parcels belong to the ones that are arriving in the West of the anticyclone (according to our definition) which we will investigate closer in Figure 9e.

Similar airstreams were observed in the DL (Figure 6c,d) with the exception that the airstream coming from the polar regions is more important than in the BL. Some air-parcels in this airstream were advected once around the whole Arctic before ente-

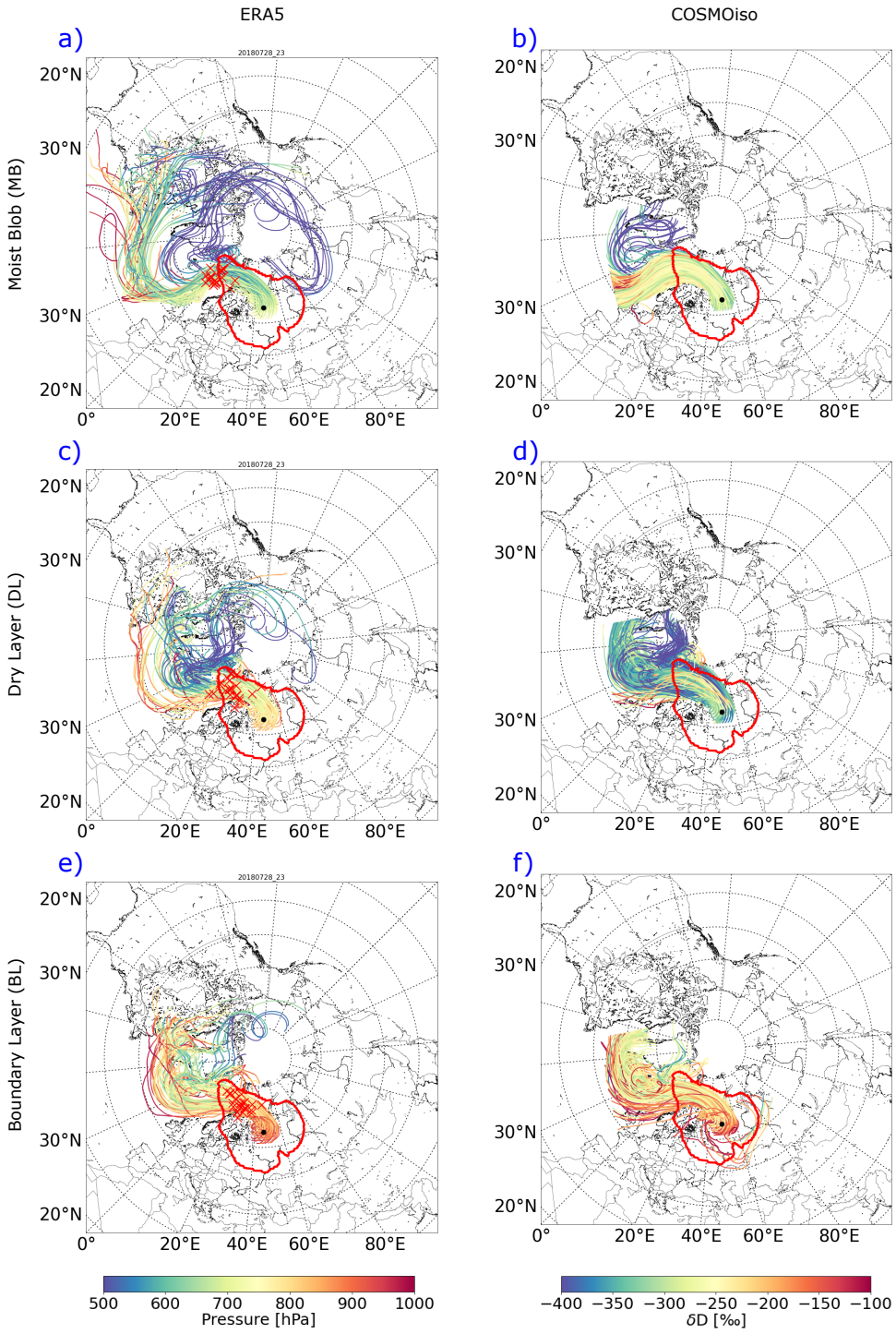

Figure 6: The left column shows the ten-days backward trajectories, that arrived at 23 UTC on 28 July 2018, calculated with the ERA5 reanalysis data and colored with the pressure. The red crosses indicate the location of the air-parcels two days before arrival for every tenth trajectory. The right column shows the eight-days backward trajectories calculated with the $\text{COSMO}_{\text{iso}}$ model and colored with the δD signal. For ERA5 and $\text{COSMO}_{\text{iso}}$ only every third trajectory was plotted for a better clearity. The red contour shows the anticyclone mask.

ring the anticyclone. This shows us that the air in the DL generally originated at locations further poleward than in the BL. Interestingly, a smaller airstream was advected from the warmer southern regions (about 52°N) and mixed with this polar air before entering the anticyclone.

In the MB (Figure 6a,b) it stuck out that the main airstream originated from regions much further south (about 40-50°N) than it was the case in the BL and DL. These trajectories ascended very strongly until their arrival in the MB in the center. Other than that, the airstreams in the MB were similar as for the other two vertical layers but they generally experienced larger horizontal advection during the last ten days than in the BL and DL.

Center moisture sources

Beside the trajectory pathways we are also interested to understand where the moisture transported in these airstreams originated from. Therefore, the MSD tool (Section 5.4, Sodemann et al. (2008)) was used which shows us the percent share of the moisture that was taken up at a certain location to the total moisture of an air-parcel at its arrival in the center. Figure 7 shows us the MSD for the three vertical levels in the center (BL, DL, MB) for ERA5 (left column) and $\text{COSMO}_{\text{iso}}$ (right column). The moisture sources of the ERA5 and the $\text{COSMO}_{\text{iso}}$ agree quite well but sometimes the ERA5 shows an additional moisture source which can be explained by the limited domain of the $\text{COSMO}_{\text{iso}}$ simulation.

The most important moisture source in the BL (Figure 7e,f) is in the center where moisture was taken up by moisture exchange with the surface during the descent. The ERA5 and especially the $\text{COSMO}_{\text{iso}}$ show an additional moisture source close to Iceland where one of the airstreams strongly descended and apparently took-up moisture by moisture exchange with the oceanic surface.

In the DL (Figure 7c,d), the most important moisture source is also found in the center because the air in the DL is partly coming from cold, polar regions with low-humidity air (Figure 6c) and had no contact with the ocean surface before descending in the anticyclone center. It is expected that the air took-up moisture from the BL below via moisture exchange. Nevertheless, some moisture was also taken up in the North-Atlantic, around Iceland and near the Norwegian coast where we observed a descending airstream.

Finally, the moisture sources of the MB (Figure 7a,b) lie much further south (about 50°N) and are located in warmer and more humid regions than for the BL and DL (about 60-70°N according to Figure 7c-f). Moisture was taken up during almost the whole pathway to the anticyclone center. This difference in origin between air-parcels in the BL and DL (more poleward, colder and drier) and the MB (more southerly regions, warmer, more humid) can explain this local increase in moisture in the MB region in the center.

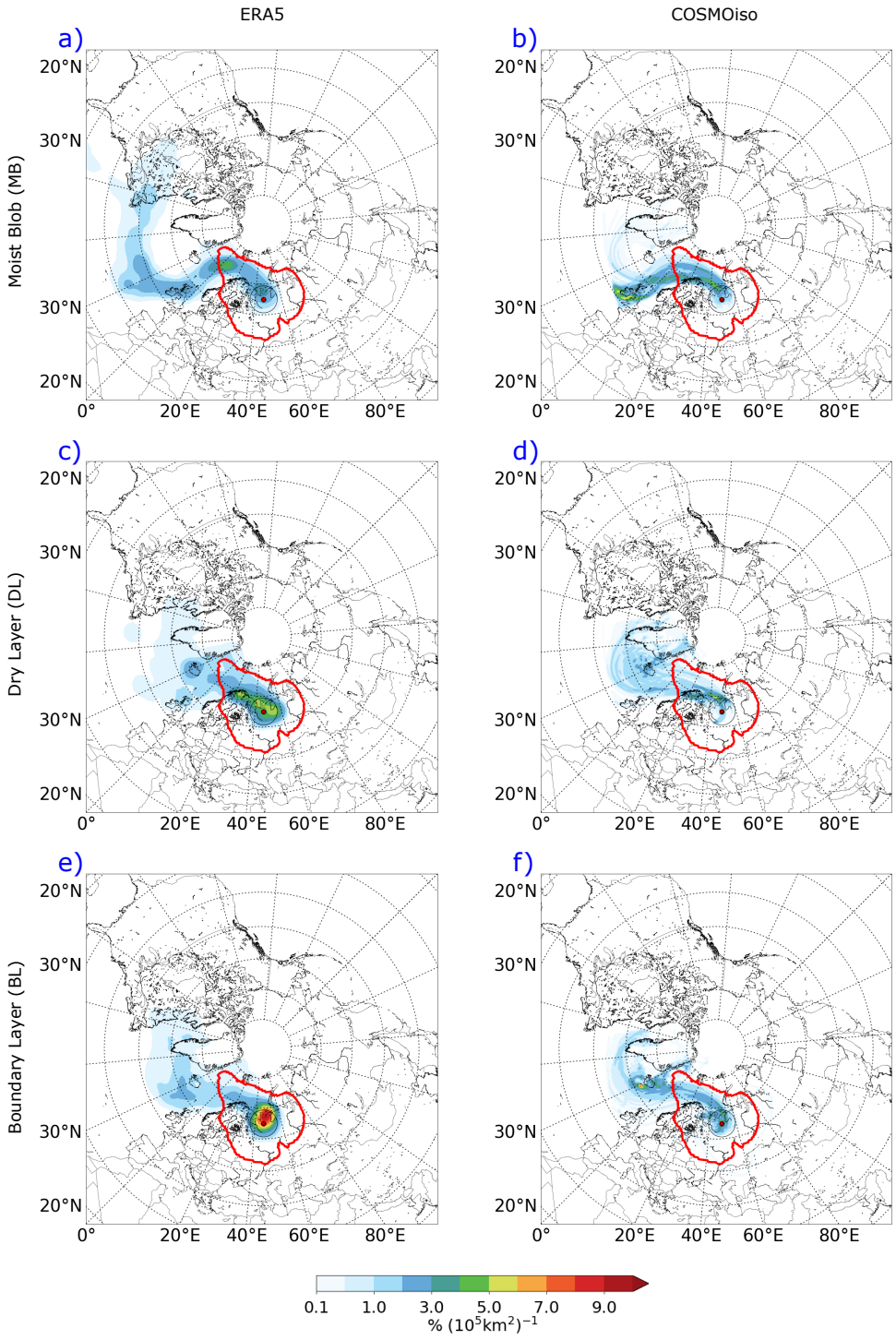

Figure 7: The left column shows the MSD of the ten-days backward trajectories calculated with the ERA5 reanalysis data according to Wernli and Schwierz (2006) and Sprenger et al. (2017) (see Section 5.3). The right column shows the MSD of the eight-days backward trajectories calculated with the $\text{COSMO}_{\text{iso}}$ model. The red contour shows the anticyclone mask.

Eastern edge backward trajectories and moisture sources
In a next step, we will look at the origin of the air and its moisture from air-parcels arriving in the eastern edge region of the anticyclone. Figure 8 shows the corresponding trajectories (left column) and the MSD (right column). Between 900-1000 hPa we see two main airstreams (Figure 8e). One originated in the West at about 60°N while another one was advected from the East outside the anticyclone and spun once around the anticyclone, before it arrived in the East inside the anticyclone. Overall, both airstreams descended strongly before they arrived.

In the MSD between 900-1000 hPa (Figure 8f) it is visible that the airstream originating from the East carried more moisture into the eastern edge region than the one from the West. This is because the eastern airstream moved on low altitudes and could therefore take up more moisture by surface exchange than the western airstream that travelled at high altitudes. The moisture source peaks close to the eastern edge region where the trajectories of both airsterams strongly descended.

Between 750-850 hPa we see similar trajectories and moisture sources (Figure 8c and Figure 8d respectively) as for 900-1000 hPa, but we have an additional airstream from the North (75-80°N). This airstream brings cooler and also drier air into the anticyclone which might explain the decrease in specific humidity compared to the layer below (Figure 5). This airstream, coming from the Greenland ice sheet, has an important moisture source along the coast of Greenland where it descended and took up moisture when it reached the open ocean (Figure 8f).

On 500-700 hPa we see that we have even more trajectories coming from the colder and drier regions further north (Figure 8a), explaining why the air gets drier with increasing altitude in the eastern edge region. The main moisture source comes therefore again from the eastern airstream (Figure 8b) that originates in warmer, more humid regions. Additionally, we see some single air-parcels entering the anticyclone from the South (Figure 8a,b) that also transport some moisture into the eastern edge region.

Western edge backward trajectories and moisture sources
Finally, we will look at the trajectories and moisture sources of the western anticyclone edge (Figure 9). At 900-1000 hPa we see three airstreams (Figure 9e). The largest airstream entered the anticyclone from the West but instead of being advected clockwise around the center, this airstream was directly distracted to the western edge region where it descended. Another airstream was advected around the anticyclone center from the East while it moved quite far south (about 45°N) on its way to the western anticyclone edge region (Figure 9e). This airstream descended strongly some days before its arrival and picked up moisture close to the surface (Figure 9f). Another small airstream entered the anticyclone at high altitudes in the South and then strongly descended until its arrival (Figure 9e).

Between 750-850 hPa we see similar airstreams as for the layer below (Figure 9c) but the influence from the southern airstream gained on importance. Additionally, the airstream originating in the East moved further south (about 40°N) than it was

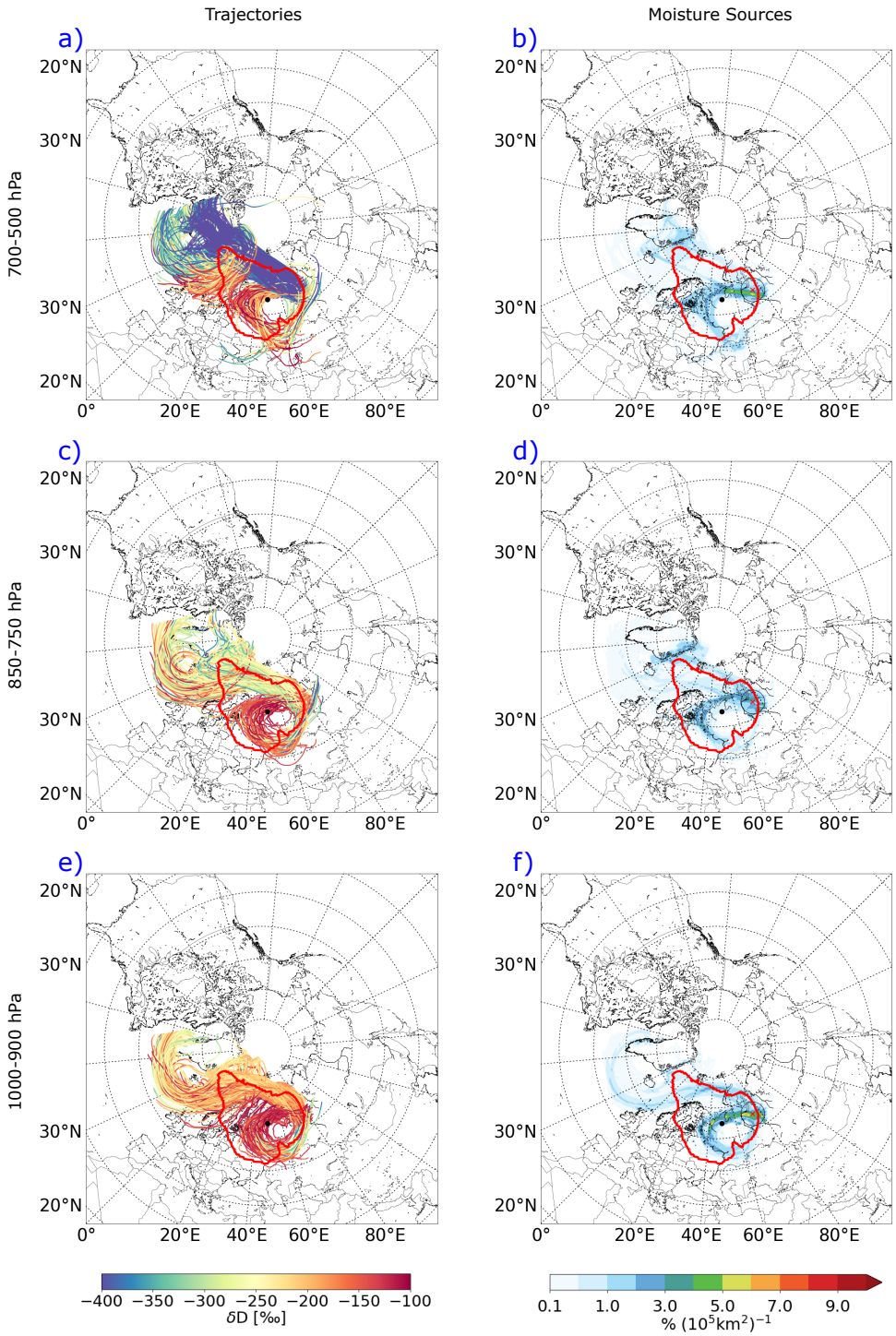

Figure 8: The left column shows the eight-days backward trajectories, that arrived at 23 UTC on 28 July 2018, calculated with the $\text{COSMO}_{\text{iso}}$ model for the eastern anticyclone region (definition, see Section 5.3) and colored with the δD signal. Only every third trajectory was plotted for a better clearity. In the right column the MSD of the trajectories is shown. The red contour shows the anticyclone mask.

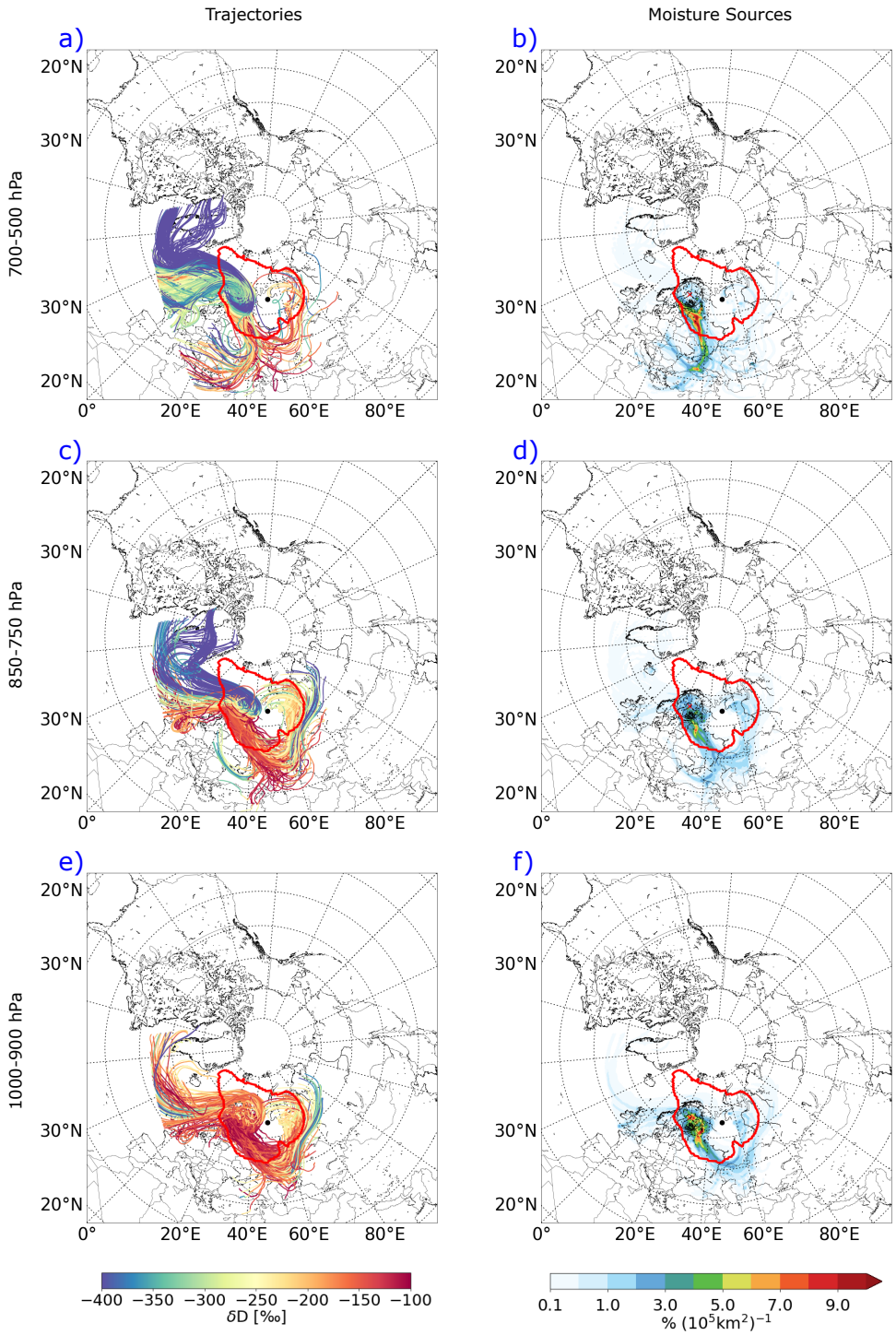

Figure 9: The left column shows the eight-days backward trajectories calculated with the $\text{COSMO}_{\text{iso}}$ model for the western anticyclone region (definition, see Section 5.3) and colored with the δD signal. Only every third trajectory was plotted for a better clearity. In the right column the MSD of the trajectories is shown. The red contour shows the anticyclone mask.

the case on the lower pressure levels, leading to an enhanced moisture transport from the warmer and more humid South into the western part of the anticyclone (Figure 9d). As this air has its origin in warmer and more humid regions than the air in the eastern edge region on the same pressure level, we see more humidity in the western edge region than in the eastern edge region.

Between 500-700 hPa we observe that the airstream originating from the East lost on importance (Figure 9a). Instead, most trajectories enter the anticyclone from the West and the South. While the trajectories from the West do still not contribute much to the moisture in the anticyclone (Figure 9b), the trajectories entering the anticyclone in the South form a major moisture source. This airstream originated in warmer and more humid regions.

Summary of the general circulation at 23 UTC on 28 July 2018
This Lagrangian analysis (backward trajectories and MSD) gave us helpful insights into the general circulation of this anticyclone at 23 UTC on 28 July 2018. We can conclude that for this specific day the inflowing air mainly originated in the West because the anticyclone blocked the westerly jet stream. Due to the clockwise circulation of the anticyclone, the air entered the anticyclone in the North. The inflowing air consisted out of two to three different airstreams (depending on the altitude one is looking at), some of them ascended and some descended while they entered the anticyclone (Figure 6).

The air that was advected close to the anticyclone center descended while it twisted clockwise around the core (Figure 6). During its descent close to the center it warmed adiabatically. As warmer air can hold more moisture than cold air, the relative humidity of the descending air decreased and the center was visible as a cloud-free region. In contrast, the outside of the anticyclone was covered by clouds which appeared as a cloudy ring around the anticyclone center. This air in the center experienced only small horizontal but large vertical movement compared to the air closer to the anticyclone edge.

Moreover, we clearly see different origins of the air-parcels arriving in the center (Figure 6). Air-parcels in the MB came from warmer and more humid regions in the South, while air-parcels in the DL came from colder and drier regions in the North. This lead to the vertical structure that we saw in Figure 5 with a humid surface, a dry layer above and again a moist layer on top of the dry layer. Air-parcels in the BL picked up moisture from the surface, diverged from the core, while they still turned in a clockwise direction, and moved towards the edge of the anticyclone. This air was then influenced by the circulation along the edge of the anticyclone.

The air along the edge also turns in a clockwise direction around the center but with a much larger radius. In the East, it descends very strong and moves to the South and further to the West along the anticyclone edge. We sometimes also see that some air from outside enters the anticyclone in the Southeast and South. Some of this air (usually the one that entered more in the Southeast) is entering the descending

circulation close to the center while some air (usually the air that entered more in the South) is advected to the western anticyclone edge. This air usually brings in warm and moist air, which leads to the observed spiral-shaped structure in specific humidity and temperature, as we have seen in Figure 3.

In the West, the air ascends along the anticyclone edge and forms some clouds when it reaches saturation due to the adiabatic cooling during its ascent. Finally, some of the air at the western edge is leaving the anticyclone by ascending and moving to the Northeast, out of the anticyclone.

In short, we can say that we have two main pathways of how air is circulating in the anticyclone. First, we observe a ring-like circulation close to the core. Here the air descends strongly independent of its location relative to the center while circulating clockwise around the core. Second, we observe another circulation around the core with a much broader radius along the anticyclone edge. Here, the air mostly follows the isentropes. The isentropes rise towards the pole and sink towards the (sub)tropics. Therefore, we see sinking air to the East and rising air to the West of the anticyclone center.

6.2.3 Isotope analysis

After we investigated the circulation and the moisture sources in more detail, we want to investigate the isotopic structure and its related moisture processes in a next step. Therefore, we look at the same vertical cross section as we did in Figure 5a but this time for the stable water vapour isotopes. Figure 10 shows the vertical zonal (from East to West) cross section through the anticyclone center colored with the δD signal.

The first thing that stands out in Figure 10 is that we see the vertical three layer structure in the center again. The MB is clearly visible at around 500-700 hPa (pink dashed circle). It is characterized by a higher δD compared to the δD on the same altitude regions east and west of it. The center of the MB is situated at around 650 hPa and shows a value of about -200‰. Below the MB in the center, at around 800 hPa (orange dashed circle), we observe a very low δD signal compared to the areas above and below it. The δD decreases here to a value of about -260‰ and is situated at the location of the DL. Right below the DL, we see that the δD in the BL is enhanced again (yellow dashed circle). Moreover, we see that the δD is generally higher close to the surface and decreases steadily towards higher altitudes at the eastern and western edge. In the West the δD signal is higher than in the East on the same altitudes.

To understand, why we observe this isotopic signal in the anticyclone, we will look at the $\text{COSMO}_{\text{iso}}$ trajectories (colored with the δD signal) from Section 6.2.2 again. Figure 6, Figure 8 and Figure 9 will help us to interpret the isotopic signal and link it with the dynamics, circulation and moisture transport of the anticyclone.

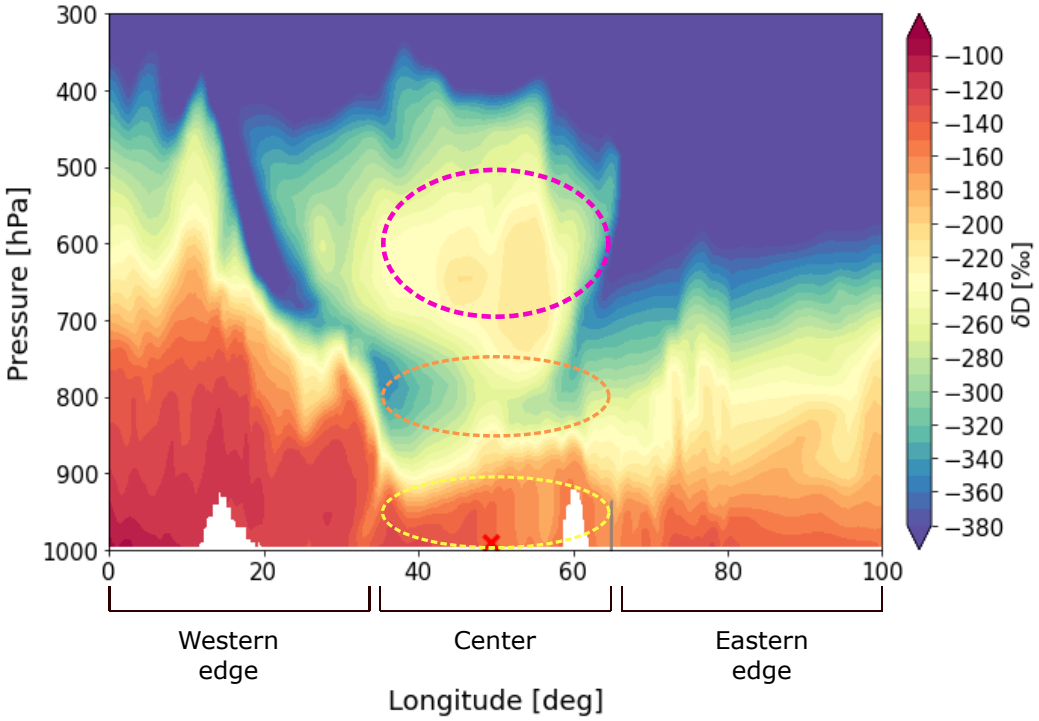

Figure 10: Vertical cross section through the anticyclone center from 0-100°E and 300-1000 hPa, showing the δD signal simulated with the $COSMO_{iso}$ model. More redish values are more isotopically enriched while more blueish values are more depleted in heavy isotopes. Figure 4 shows the exact location of this zonal cross section (black line). The red cross shows the location of the anticyclone center for the $COSMO_{iso}$ model. The pink dashed circle indicates the MB, the orange dashed circle the DL and the yellow dashed circle the BL. Along the x-axis the regions are labeled.

Isotopic signal of the trajectories arriving in the center

We saw in Figure 6e,f that the two main airstreams arriving in the MB came from southerly regions and that they show an enriched δD signal at around -220‰. In contrast, the main airstream in the DL (Figure 6c,d) originated more poleward and shows a more depleted δD signal. This fits well with our observation from Figure 10.

Generally, we expect that the regions more poleward are more depleted in heavy isotopes than the regions closer to the tropics. This is because the water vapour, that evaporated in the mid-latitudes, is transported towards the pole by the global atmospheric circulation. On its way, preferentially heavy isotopes are rained out (see Section 2) which leads to a more depleted signal in the more poleward regions compared to the regions closer to the (sub)tropics (fractionation).

Another factor that is important for the isotopic signal of an air-parcel is its altitude. Generally, trajectories on a high altitude show a more depleted δD signal as they lost preferentially heavy isotopes during cloud formation and rain-out but they could not

take up new heavy isotopes via surface moisture exchange or evaporation. This can for example been shown for the trajectories arriving in the MB. These trajectories showed a strong ascend of about 400 hPa about 100 to 75 hours before their arrival. During this ascent the air cooled and saturated and lead to cloud formation and precipitation. The precipitation decreased the δD signal, as preferentially heavy isotopes were rained out.

Additionally, we see another phenomenon in the BL that strongly influenced the δD signal. The airstreams arriving in the BL descended strongly in the center and moistened close to the surface. This surface moisture was enriched in heavy isotopes and therefore increased the δD signal in the BL.

Isotopic signal of the trajectories arriving in the eastern edge region
We have seen in Figure 8f that the moisture between 900-1000 hPa in the eastern edge region was mainly transported by the airstream originating from the East. These trajectories increased their isotopic signature while they descended and took up isotopically-enriched air via surface exchange (Figure 8e) as we have already seen it in the center before.

Between 750-850 hPa we saw another moisture source along the coast of Greenland (Figure 8d). This air is very depleted in heavy isotopes due to its northern location (Figure 8c) and therefore reduces the δD signal in this layer compared to the layer below (900-1000 hPa). The same can also be seen for the 500-700 hPa pressure level.

Isotopic signal of the trajectories arriving in the western edge region
In Figure 9c,e we saw that the trajectories in the layer between 900-1000 hPa and 750-850 hPa came from about 40-45°N, so from a region further south than the trajectories that arrived in the eastern edge region. This explains why the δD signal in the West is more enriched on these pressure levels than in the East. Towards the 500-700 hPa level the δD signal gets more depleted (Figure 10) because the airstream entering the anticyclone from the South gains on importance and brings some more depleted air into the western edge region (Figure 9a).

The knowledge we gained about the vertical structure of the moisture and isotopes in the anticyclone will help us now to better understand the δD signal of the whole atmospheric column, the so called column integrated δD signal. This is the isotopic signal that the satellite-based instrument TROPOMI measures and which we want to better understand in this Master's thesis.

Figure 11 shows the column integrated δD signal that was calculated with the $\text{COSMO}_{\text{iso}}$ model for 09 UTC on 29 July 2018. Note that for this analysis not 23 UTC on 28 July 2018 was chosen because the satellite with the attached TROPOMI orbits the Earth during the course of the day and therefore does not cover our area of interest continuously. 09 UTC on 29 July 2018 was the closest timestep where we had data from the TROPOMI over Scandinavia and the Russian Arctic.

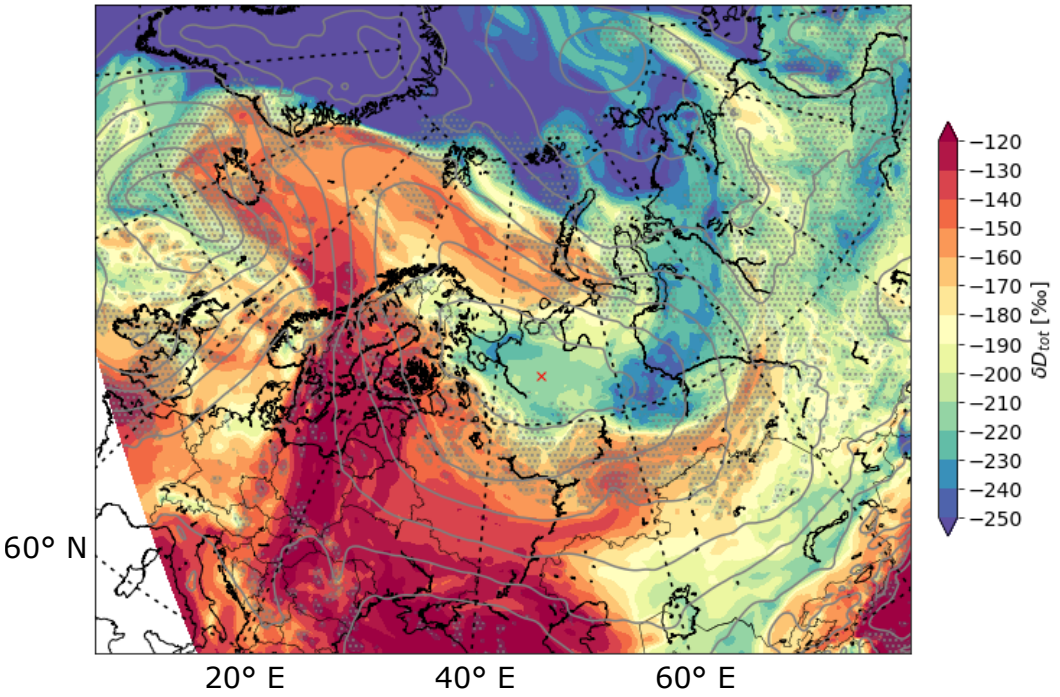

Figure 11: Total column integrated δD signal from the $\text{COSMO}_{\text{iso}}$ model for 09 UTC on 29 July 2018.

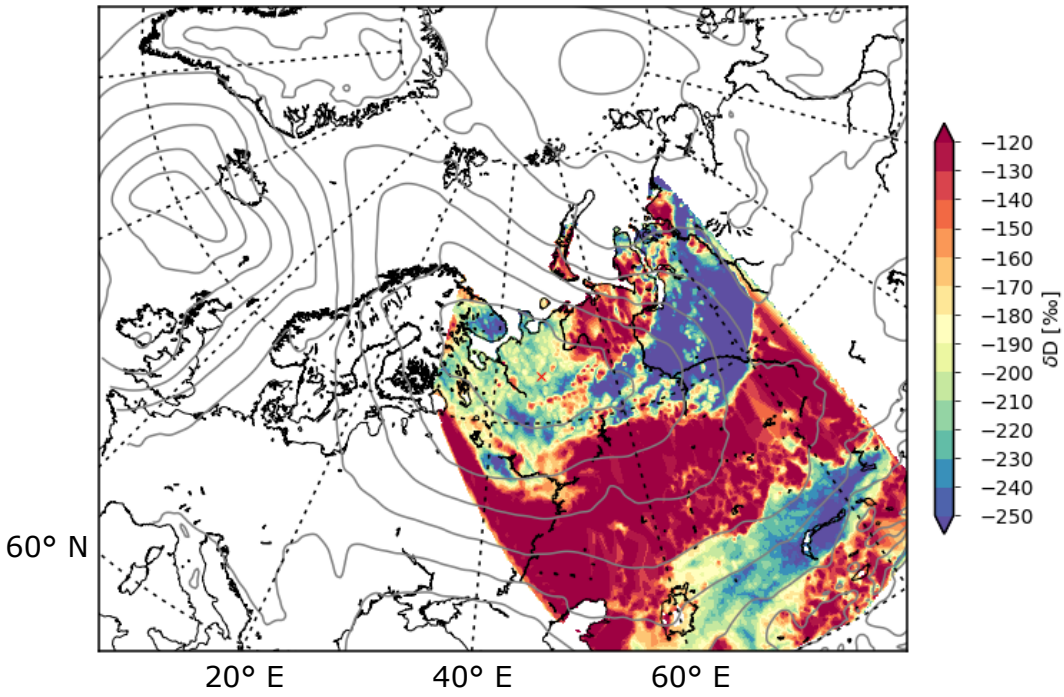

Figure 12: Total column integrated δD signal as retrieved by the satellite-based TROPOMI for 09 UTC on 29 July 2018.

We can observe a clockwise twisting, spiral-shaped δD signal as we have already seen it in Section 6.2.1 for the temperature and specific humidity (Figure 11). As explained earlier, we expect the air further north to be generally more depleted in heavy isotopes than the air in the South. According to the modelled isotopic total column signal, the northern and southern air masses differentiate by about 130‰. This spiral, twisting clockwise around the center, can also explain the higher δD values in the western edge region compared to the eastern edge.

Further, we observe that the region in the East is even more depleted than the center itself. With our knowledge about the vertical isotope structure we know now that the center is influenced by the MB that increases the total column δD signal in the core but in contrast, in the East, where we do not have a MB and about the same amount of specific humidity in the BL as in the center (Figure 10), the δD signal is decreased.

To end the description of this specific timestep, we will finally look at the TROPOMI column integrated δD signal (see Figure 12) and compare it with the $\text{COSMO}_{\text{iso}}$ column integrated δD (Figure 11) to see how well the model fits with observational data. As the TROPOMI only measures over land and in cloud-free regions, we have only partial coverage in Figure 12.

We see that the general distribution of the heavy and light stable water vapour isotopes in the TROPOMI fits quite well with the distribution in the $\text{COSMO}_{\text{iso}}$ model. We observe a spiral-shaped δD signal in the TROPOMI data that recurves clockwise around the center (Figure 12). Moreover, the isotopic signal from the North is more depleted than the one in the South. We also observe that the center (about -190‰) is less depleted than the region in the East (less than -250‰) due to the MB in the center.

Nevertheless, the TROPOMI shows a much more depleted signal east of the center than the $\text{COSMO}_{\text{iso}}$ (more than 30‰ difference) while the signal in the center seems to be about 20‰ lower in the $\text{COSMO}_{\text{iso}}$. The air with the enhanced δD signal (about -120‰) in the South is more enriched in the TROPOMI by about 10-60‰ and covers a much larger area compared to the $\text{COSMO}_{\text{iso}}$. Furthermore, it seems that the spiral is slightly shifted southward in the TROPOMI compared to the $\text{COSMO}_{\text{iso}}$ as some of the strongly depleted air from the East was advected south of the anticyclone center and the more enriched air in the North reaches a little further south.

To conclude this comparison between the model and observational column integrated isotopic signal we can say that the general isotopic features are very similar between the $\text{COSMO}_{\text{iso}}$ and the TROPOMI but the TROPOMI shows higher (lower) values for the strongly isotopically enriched (depleted) regions. From this analysis it is difficult to say which of the two signals represents the real state better. The TROPOMI might have measurement uncertainties as it shows only few gradations between the very enriched (-120‰) and very depleted (-250‰) signal, in the range where most of the values lie in the $\text{COSMO}_{\text{iso}}$ simulation. It would be nice to also

have values over ocean, to better understand the northern anticyclone region with the TROPOMI data and in cloudy regions, to better understand the western edge of the anticyclone. On the other hand the $COSMO_{iso}$ model might have errors as well because of uncertainties in the model simulated meteorology.

6.3 Anticyclone-centered perspective

We learnt a lot about the moisture structure, the circulation and the isotopic distribution in the anticyclone for 23 UTC on 28 July 2018. In a next step we want to find out if these characteristics can be found during the whole July 2018 event. We saw in Section 2 that the spiral-shaped structure in the temperature and specific humidity can be observed over the whole event. At some days it is better visible than on others when for example the anticyclone gets disturbed by the merging of a second anticyclone.

In the following, we want to find out if the three layer structure in the center is visible over the whole event and if the edge regions behave similar as for 23 UTC on 28 July 2018. To do so, we used an anticyclone-centered perspective that shows us the state of the anticyclone with respect to its core, independent of its location on Earth. Figure 13 shows the anticyclone-centered vertical zonal cross section through the center that was averaged over the July 2018 event. 0 indicates the location of the anticyclone core. The definition of the center and the eastern and western edge region (as labelled in Figure 13) is only an approximation because the zonal extension of the anticyclone varied over the whole event.

We see, as is was the case for 23 UTC on 28 July 2018, that the moisture content is largest close to the surface and that we see about 2 g kg^{-1} more moisture in the BL in the West than in the East and in the center (Figure 13). About 40° east of the center we see a very low specific humidity at the surface. This can only be explained by an extrapolation error and will therefore be excluded for the further analysis. Moreover, the moisture decreases steadily in the East and West with increasing altitude.

What might surprise is that we do not see a MB in the center (Figure 13) and therefore also not a clear three layer structure as it was the case for 23 UTC on 28 July (Figure 5a). If we look at the center (0°) we see that the lines of constant specific humidity are further away at about 600-800 hPa than compared to the edge regions and the moisture decreases steadily with increasing altitude. This characteristics appears when we calculate a mean cross section while the MB (and accordingly also the DL below) move in altitude over the event. The MB and DL are smoothed out. Only at around 780 hPa we observe a small local decrease in specific humidity due to the DL that might have been located often a little above or below this height and therefore marked this altitude with a locally reduced humidity structure. Additionally, if we look at vertical cross sections from different timesteps during the event, we see at most days a clear three layer structure in the center (not shown), supporting our findings from Sections 6.2.

Instead of a MB it seems as if we would have a dry blob at around -10° in the center (Figure 13). This dry blob is most likely the result of the recurving cold and dry airstream from the East that originally originated in the more northerly regions. The location of this dry blob fits well with the location of the cold and dry air west of the MB that we have seen in Figure 5a.

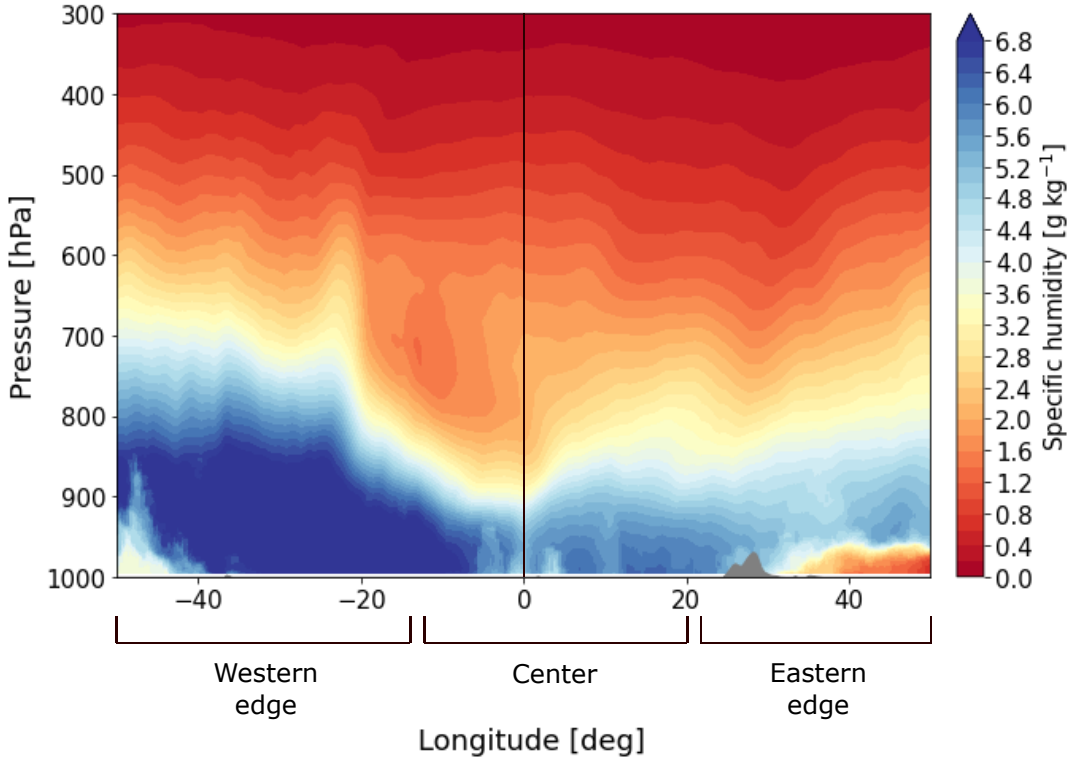

Figure 13: Mean zonal vertical cross section of the specific humidity through the core of the anticyclone. The mean cross section was calculated from 00 UTC on 20 July 2018 to 23 UTC on 29 July 2018 while the 25 and 26 July were excluded due to the moisture intrusion into the center from Southwest at these two days (see Section 2). The vertical line indicates the location of the core (0° longitude). The x-axis indicates the longitudinal distance (in deg) from the core. Negative values indicate regions located west of the core, positive values indicate regions east of the core.

Although the MB and the DL were smoothed out in Figure 13 we want to know if we can see a difference in the origin of the air and moisture on different altitudes in the center. Thus, averaged trajectories over each day of the event were calculated for the BL, DL and MB with the $\text{COSMO}_{\text{iso}}$ (Figure 14).

We see that the air in the MB (Figure 14a,b,c) generally came from more southerly regions (about -15° to -10°) than the air in the DL (Figure 14d,e,f, -15° to 0°). Moreover, the region of origin of the MB was generally more humid and isotopically enriched than in the DL (see Figures 14b,e and 14c,f). The air in the BL is more humid and more enriched in δD at its arrival in the center than in the DL and MB (Figure 14h,i).

Nevertheless, we do not really see that the air arriving in the MB is more humid than in the DL (Figures 14b,e) and also the δD signal is not clearly higher (Figures 14c,f). This can happen when the MB and the DL overlap during averaging because they changed their altitude during the course of the event.

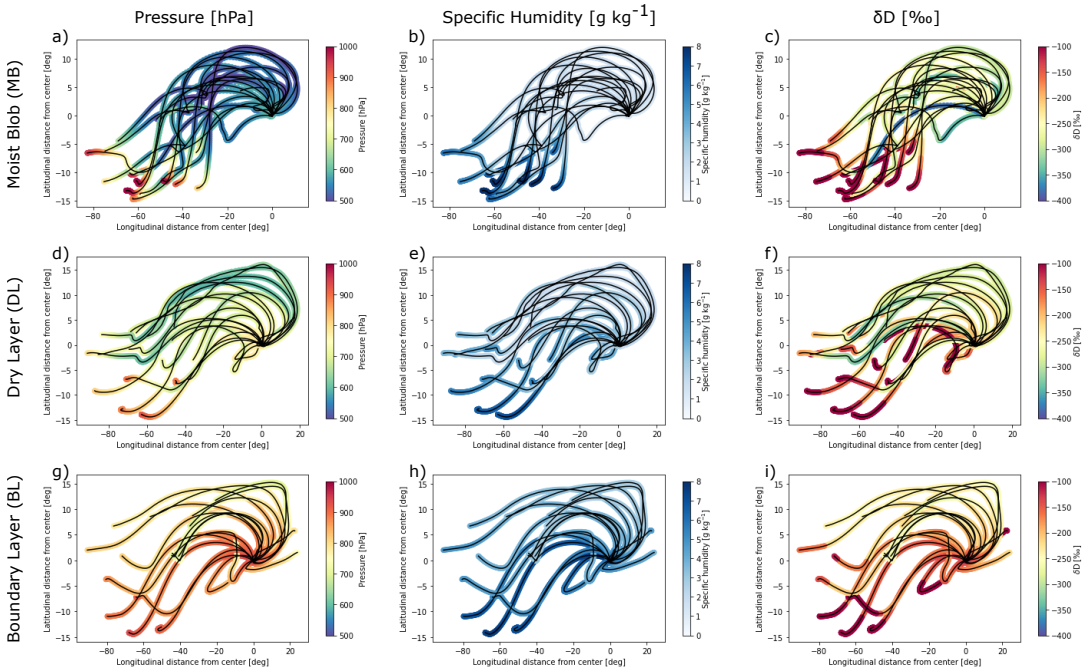

Figure 14: Anticyclone-centered averaged trajectories for each day of the event (in total 19 trajectories) arriving in one of the corresponding vertical layers (BL, DL or MB) in the center of the anticyclone. 0 indicates the location of the core. The x-axis shows the longitudinal distance from the core. The y-axis shows the latitudinal distance from the core. The left column is colored with the pressure, the middle column with the specific humidity and the right column with the δD signal.

After this anticyclone-centered Lagrangian perspective on the event we will finally investigate the isotopic structure of the anticyclone. Figure 15 shows the same averaged cross section through the center as Figure 13 but colored with the δD signal. As we have already seen in Figure 13 we can also not see a clear MB in the center in Figure 15 because the MB and the DL are smoothed out but we observe a depleted blob at about -10°. This depleted blob is most likely the result of the recurving depleted airstream from the East that originally originated in the more northerly regions. Moreover, we see that the surface is enriched in heavy isotopes while it gradually decreases with increasing altitude along the eastern and western edge. At about 40° east of the center we see a very enriched isotopic signal at the surface. As already described in Figure 13 this is most likely an extrapolation error.

Surface isotopic signal

In Figure 13 and Figure 15 we saw that the surface layer has an important influence on the total column δD signal as it contains an important share of the moisture stored in the whole atmosphere. Therefore, we want to investigate how the surface isotopic signal changes between different locations in the anticyclone before examining its importance for the column integrated δD signal later.

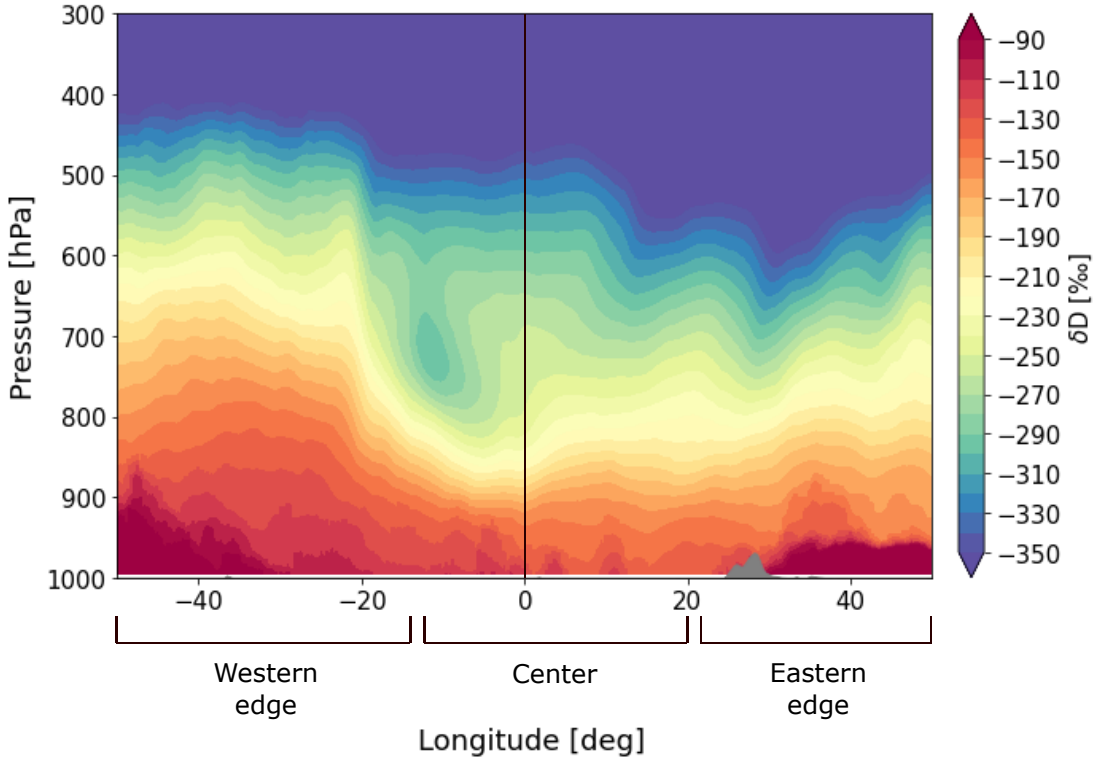

Figure 15: Mean zonal vertical cross section of the δD through the core of the anticyclone. The mean cross section was calculated from 00 UTC on 20 July 2018 to 23 UTC on 29 July 2018 while the 25 and 26 July were excluded due to the moisture intrusion into the center from Southwest at these two days (see Section 2). The vertical line indicates the location of the core (0° longitude). The x-axis indicates the longitudinal distance (in deg) from the core. Negative values indicate regions located west of the core, positive values indicate regions east of the core.

Figure 16 shows the anticyclone-centered δD signal at 950 hPa averaged over the whole July 2018 event (00 UTC on 15 July 2018 until 23 UTC on 02 August 2018) and calculated with the $\text{COSMO}_{\text{iso}}$ model. We observe a clear spatial pattern in the surface isotopic signal that follows a spiral-shaped structure again. The air to the West of the center is much more enriched in heavy isotopes than the air in the Northeast and East. This can be explained, as in Section 6.2.3, due to the generally more enriched air in the South compared to the North, that is advected clockwise around the anticyclone. The center on the other hand seems to be influenced by both isotopic signals and shows a medium isotopic signal at around -130‰.

In a next step, we will compare this model-generated surface isotopic structure with the ground-based isotopic measurements from the Finnish weather station in Pallas. Figure 17 shows the δD and specific humidity timeseries over the July 2018 blocking event measured in Pallas.

We observed that Pallas was close to the anticyclone core at 23 UTC on 27 July 2018 (green vertical line in Figure 17) and moved towards the northwestern anticyclone

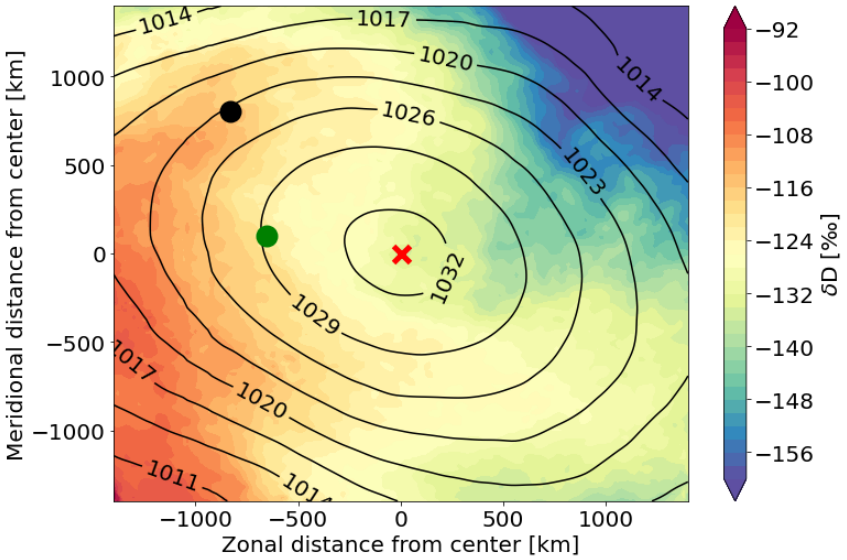

Figure 16: Mean anticyclone-centered δD signal at 950 hPa over the whole July 2018 blocking. The red cross shows the location of the anticyclone center. As the anticyclone center changed its location over Earth strongly during the whole event, the surface δD signal is shown here with respect to the anticyclone core. The green (black) circle shows the location of Pallas relative to the core at 23 UTC on 27 July (19 UTC on 30 July) when the δD signal in Pallas was strongly reduced (enhanced).

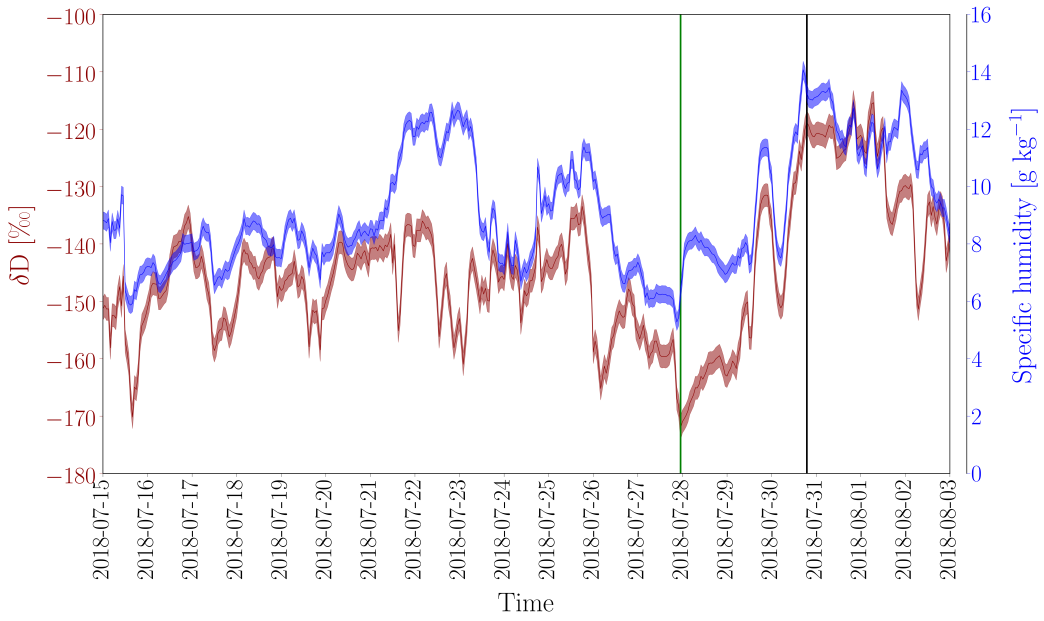

Figure 17: The δD (red curve) and specific humidity (blue curve) timeseries measured at the ground weather station in Pallas (Finland) for the July 2018 blocking event. The green vertical line indicates 23 UTC on 27 July 2018 (minimum in δD) and the black vertical line indicates 19 UTC on 30 July 2018 (maximum in δD).

edge until 19 UTC on 30 July 2018 (black vertical line in Figure 17). The locations relative to the anticyclone core are colored in Figure 16 with green and black dots accordingly. The observational data from Pallas fits quite well with the model output from Figure 16. We see a more depleted δD signal when Pallas is closer to the center (green line/dot) than compared to the time when Pallas is closer to the northwestern anticyclone edge (black line/dot).

In between these minimum (green line) and maximum (black line) isotopic values the δD signal in Pallas (Figure 17) increased steadily with one more peak at 21 UTC on 29 July 2018. This was the time when Pallas reached the isotopically enriched northwestern edge but experienced shortly after again the influence of the center before the δD finally reached its maximum value a few hours later (black line). A similar behaviour is observed in the specific humidity with a reduced signal at 23 UTC on 27 July 2018 and a higher signal at 19 UTC on 30 July 2018.

Although the isotopic signal between the model and the observational data seems to fit quite well after this first rough investigations, we see that the difference in δD is only small in Figure 16 between the two locations of Pallas (green (about -122‰) and black (about -118‰) dot) while the measurements in Pallas (Figure 17) indicate a larger difference in the surface isotopic composition (about -170‰ and -115‰). This difference can be explained because the modelled anticyclone-centered low-level δD signal (Figure 16) is a mean over the whole blocking event while Figure 17 shows the instantaneous isotopic signal at each day. We can therefore expect that the isotopic signal in the core and in its near surrounding at 23 UTC on 27 July 2018 (green line/dot) was more depleted than indicated by the model-generated mean anticyclone-centered plot. This is exactly what we see in the low-level isotopic signal modeled with the $\text{COSMO}_{\text{iso}}$ model for 23 UTC on 27 July 2018 (not shown).

To conclude, we can say that beside the MB also the surface isotopic signal might play an important role in influencing the total column δD signal, as it shows large variations depending on its location relative to the anticyclone core. Moreover, the surface layer and the MB are the regions with the largest specific humidity values and it is therefore very likely that both of them strongly influence the total column isotopic composition. To check for this, we will in the following investigate the total column δD signal for the July 2018 event, first with the $\text{COSMO}_{\text{iso}}$ model and after with the observational data from the TROPOMI.

Total column integrated δD signal

Figure 18 shows the anticyclone-centered total column δD signal averaged over the whole July 2018 event and calculated with the $\text{COSMO}_{\text{iso}}$ model. We see that the structure of the column integrated δD signal is quite similar to the structure we have seen at 950 hPa (Figure 16), indicating that the surface isotopic signal plays a major role in defining the anticyclone-centered total column integrated signal.

We see that the region in the Southwest is stronger enriched (Figure 18) in relation to the other anticyclone regions than it was the case at 950 hPa (Figure 16). This can be explained by the fact that the western edge region contains a lot more moist-

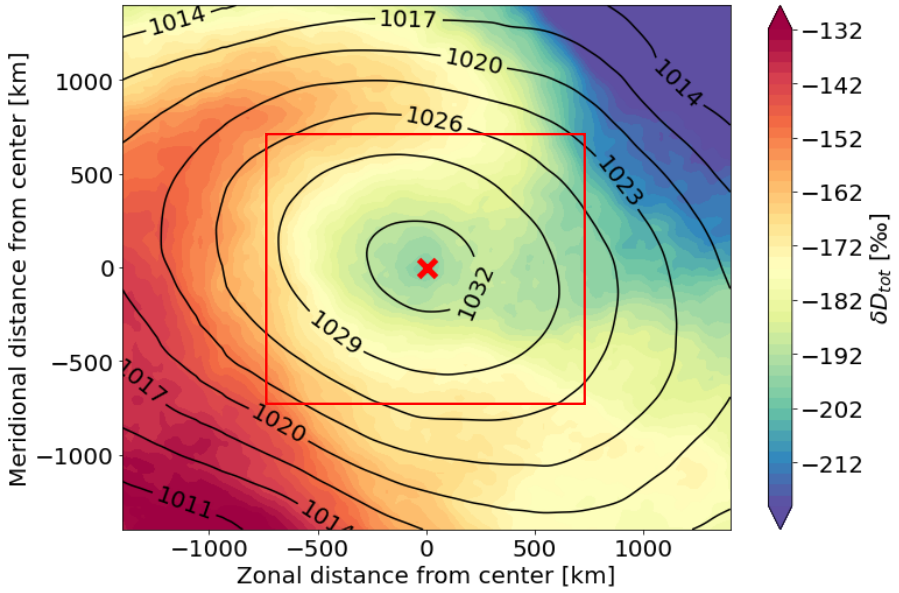

Figure 18: Mean anticyclone centered δD signal over the whole vertical atmospheric column (column integrated) calculated over the whole July 2018 blocking with the $\text{COSMO}_{\text{iso}}$ model. As the anticyclone core changed its location over Earth strongly during the whole event, the total column integrated δD signal is shown here with respect to the anticyclone core (red cross). The red rectangle indicates the domain we look at in Figure 19.

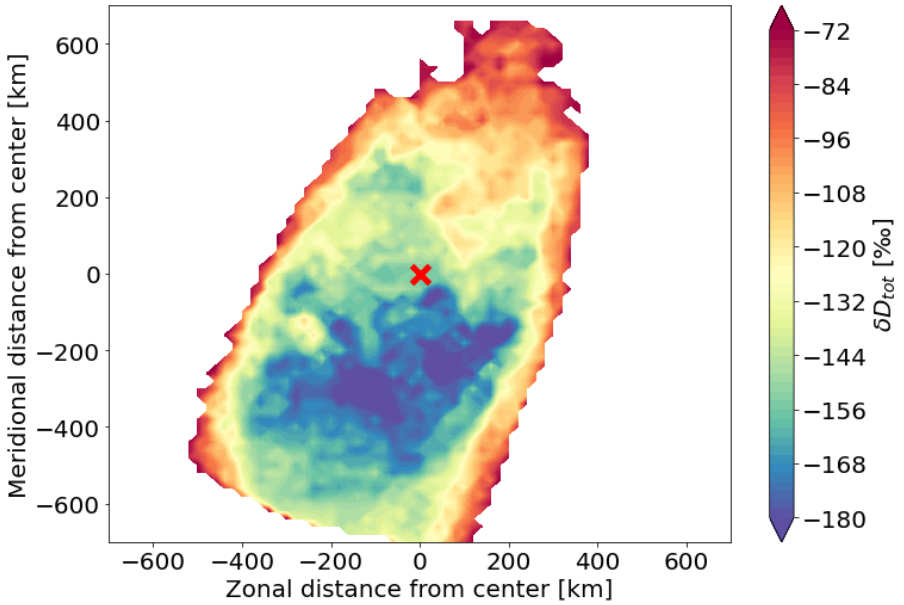

Figure 19: Mean anticyclone-centered δD signal over the whole vertical atmospheric column (column integrated) over the whole July 2018 blocking measured with the TROPOMI. As the anticyclone core changed its location over Earth strongly during the whole event, the total column integrated δD signal is shown here with respect to the anticyclone core (red cross). The domain and the colorbar is different than in Figure 18.

ure over the whole vertical column (and especially close to the surface) than the eastern edge region and the center (Figure 15). As the western edge air mostly consists out of heavy isotopes this sums up to an even more enriched signal in the total column isotopic signal.

Furthermore, we see that the center is more depleted in δD (Figure 18) in comparison to the other anticyclone regions than it was the case on 950 hPa (Figure 16). This is surprising because one might expect the center to be more enriched in δD due to the MB that increases the total column δD signal. This can be explained by the fact that the eastern and western edge region generally contain more moisture (and mainly enriched moisture) close to the surface (Figure 15) than the center which sums up to a higher column integrated δD signal along the edge than in the center. Although the MB increases the isotopic signal in the center it is not enough to increase the total column integrated δD value to a value higher than observed along the edge.

To complete the analysis of this blocking event, we will finally compare the model results (Figure 18) with observational data from the TROPOMI (Figure 19). Please be careful when comparing the Figures as Figure 19 shows a smaller area of the anticyclone than Figure 18 (red rectangle) and the colorbars are different.

Figure 19 shows the average anticyclone-centered δD signal over the whole atmospheric column measured by the TROPOMI for the July 2018 event. As the TROPOMI instrument is attached to a satellite that constantly orbits the Earth it covers Scandinavia and the Russian Arctic only about once per day during daytime and covers only a small band of the Earth surface. Moreover, it only measures over land and in cloud-free regions which further reduces the available data. Therefore, the data coverage is relatively small and will most likely not have covered the whole anticyclone (Figure 19).

Nevertheless, we see that the δD north of the core is enriched in heavy isotopes (about -80‰) while south of the core the signal is more depleted with values around -180‰ (Figure 19). The center shows an intermediate signal at around -150‰. We can identify the spiral-shaped signature in the isotopic signal too but due to the lack of measurements along the anticyclone edges the spiral form is not very determined. Surprisingly, it seems that the spiral is shifted because the depleted air south of the core is located further south in the TROPOMI data than in the $\text{COSMO}_{\text{iso}}$ simulation.

Further, it is difficult to say something about the eastern and western edge in comparison to the center and the influence of the vertical structure as we are missing data from the edge regions. Nevertheless, we see that the core shows a similar or even a slightly higher δD signal compared to the more depleted regions south of the core which could be due to the influence of the MB. Thus, the core in Figure 19 shows a higher δD signal compared to the other anticyclone regions than it was the case in the model-output in Figure 18. Moreover, comparing the absolute δD values of the $\text{COSMO}_{\text{iso}}$ and the TROPOMI we see that the $\text{COSMO}_{\text{iso}}$ is generally more depleted by about 40‰ or even more.

The observations made here fit well with the observations we already made in Section 6.2. Additionally, a small band of measurements that are at the edge to where we have no measurements in Figure 19 seems to be enriched in all regions of the anticyclone. I can not explain this with my knowledge about this blocking event which let me expect that this is most likely an artefact of the retrieval.

7 Conclusions and outlook

In July 2018 a particularly persistent anticyclone dominated the Eurasian Arctic summer and lead to a strong heatwave, forest fires, dry fields, low river stages and enhanced sea ice melt in the Russian Arctic and Scandinavia (Watts (2018), Sinclair et al. (2019)). The goal of this Master's thesis was to better understand the moisture transport associated with this especially strong blocking event. Therefore, a detailed analysis of the humidity and isotopic structure of the established anticyclone was conducted for 23 UTC on 28 July 2018 based on ERA5 reanalysis data and an isotope-enabled $COSMO_{iso}$ simulation. Later, the analysis was expanded over the whole event (00 UTC on 15 July 2018 until 23 UTC on 02 August 2018) by including an anticyclone-centered perspective.

In our analysis of the moisture and δD signature of the July 2018 Arctic anticyclone we found a spiral-like structure with moist enriched air ascending from the Southwest into the anticyclone and very depleted, dry air descending in the Northeast. The western edge region was more humid ($+2$ g kg^{-1}) and enriched ($+40$‰), especially at the surface, than the eastern edge region.

In my thesis, we also analysed the 3D structure of the July 2018 anticyclone. In the central region of the anticyclone we found a relatively persistent three layer structure with a lower tropospheric specific humidity and a δD inversion. The lowest layer is the moist and heavy isotopically-enriched BL and extends up to 900 hPa. Just above the BL we found a very dry and heavy isotopically-depleted layer (DL) while above the DL we found again a moist and heavy isotopically-enriched layer (MB).

The three layers differed in their origin of air and moisture. While the BL took up its moisture very locally from the surface in the anticyclone center, the air from the DL originated in colder, drier and more isotopically-depleted regions further north. In contrast, the air from the MB arrived from relatively warmer, more humid and isotopically-enriched regions further south. Since the air-parcels from all three layers strongly descended and adiabatically-warmed in the anticyclone center, the center appeared as a cloud-free region while along the edge a cloudy-ring was observed.

The anticyclone-centered perspective further revealed that the DL and the MB move vertically in height over the course of the event. The level of the anomalously moist layer (MB) in the lower free troposphere depends on the flow conditions and the relative location of the warm-moist airstream forming the moist anomaly and the cold-dry airstream forming the DL. If the warm-moist airstream recurves into the anticyclone center, this leads to a moist layer (MB) forming in the center. The arrival altitude of this airstream in the center varies in time. If the cold-dry airstream originating from further north dominates, the center remains dry and no moisture and δD inversion forms in the lower free troposphere.

Different than originally expected, we found out that not only the moisture in the surface layer, that follows a spiral-shaped structure too, influences the total column isotope signal but that the MB further increases the isotopic signal in the center.

Comparing the $COSMO_{iso}$ and the TROPOMI column integrated δD data we see that the δD minimum is shifted southward in the TROPOMI data. This southward shift could be due to a slight shift of the anticyclone in the ERA5 reanalysis as well as in the isotope-enabled simulation, a misrepresentation of vertical mixing in the lower free troposphere in the $COSMO_{iso}$ model or due to uncertainties in the total column δD retrieval from TROPOMI. Further, the TROPOMI instrument shows higher (lower) values for the strongly isotopically-enriched (depleted) regions than the $COSMO_{iso}$. A very enriched moist ring can be observed in the TROPOMI data at the edge of the anticyclone due to an artifact of the retrieval.

Beside these interesting findings, we still have open questions which need further investigation:

- It would be interesting to investigate if we find similar moisture features as for the July 2018 event also for other summer Arctic blockings. Concretely, it would be interesting to conduct a quasi-climatological study over several summers and different events to find out if the three layer structure in the center is also visible for other summer blocking events, how the regions east and west of the center behave and if we can see a spiral-like distribution in the temperature, specific humidity and isotopes too.

- It would be of interest to investigate why this event was so persistent. Steinfeld (2019) stated that latent heating of air-parcels that ascends in the WCB could play an important role. Air ascending in the WCB enhances the upper-level ridge (and therefore also the blocking) by transporting low-PV air to higher altitudes. It would be interesting to further investigate this latent heating of air-parcels and its influence on the isotope signal associated with the blocking event in July 2018. Moreover, it would also be interesting to see if diabatically ascending air-parcels have a stronger influence on the persistence of the blocking than air-parcels that follow the isentropes and ascend adiabatically.

- Another interesting feature would be to investigate the onset and break-up of the blocking event in more detail and maybe also link it to latent-heating and the adiabatical and diabatical transport of air-parcels to the upper troposphere.

- This Master's thesis found out more about the moisture structure of the anticyclone. In a next step it would be interesting to make a link between these moisture features of the anticyclone and the extreme weather in Scandinavia and the Russian Arctic. Was this extreme weather mainly due to the cloud-free center and the therefore enhanced solar radiation or due to the reduced precipitation? Which role does the dry core of the blocking play or was it an interplay of multiple factors?

- It would be interesting to investigate more recent summer blocking events over the Eurasian Arctic with the new TROPOMI data (Schneider et al., 2021) that also provides data over land and ocean regions covered by lower-clouds. This

is especially interesting as the TROPOMI dataset is very valuable for large-scale investigations of the isotopic signal which can not be investigated with ground-based station measurements for example.

- In the view of current global warming it would be interesting to find out if the frequency of such summer blocking events will increase in future. Pfahl and Wernli (2012) stated that rising temperatures and variations in the blocking dynamics can be crucial for regional changes of warm extremes in the extratropics. This would also be crucial to protect the population from the consequences of such events.

We saw that it is important to learn more about summertime blocking anticyclones in the Eurasian Arctic to be able to better prevent the population and nature from the dramatic impacts. Knowing about the changes in a warming climate is important especially in the light of the Arctic amplification which leads to drastic changes in the Arctic for nature, animals and people.

Acknowledgements

My special thank goes to Dr. Franziska Aemisegger for her remarkable support during my Master's thesis. Especially during these special times around COVID-19 I was very lucky to have such a reliable and helpful supervisor with whom the communication also worked perfectly fine over online and without seeing each other once in person during the whole thesis. It was very motivating to have her as a supervisor and her interest in this subject is catching. I am also very grateful for her review of the thesis and her constructive feedback.

Furthermore, I want to thank Prof. Dr. Heini Wernli for his helpful inputs and ideas and for giving us Master students an as good as possible chance, to become a part of the Atmospheric Dynamics group and get interesting insights into your work. Thanks also to the whole Atmospheric Dynamics group for your helpful inputs and interesting talks and discussions. Moreover, I would like to thank Hannah Bailey and Jeffrey Welker from the University of Oulu in Finland for providing me the very interesting isotopic dataset from the weather station in Pallas. Another thank you goes to Andreas Schneider and Tobias Borsdorff from Neatherlands Institute for Space Research for providing me the interesting TROPOMI data. I was very lucky to be able to work with this data. I would also like to thank Martin Werner from the German Alfred-Wegener-Institute for providing me the boundary conditions that were used to set-up the $\text{COSMO}_{\text{iso}}$ simulation. Further, MeteoSwiss and the ECMWF are acknowledged for providing access to the ERA5 data.

References

Aemisegger, F. (2018). On the link between the North Atlantic storm track and precipitation deuterium excess in Reykjavik. *Atmos. Sci. Lett.*, 19(12):e865. doi:10.1002/asl.865.

Aemisegger, F., Pfahl, S., Sodemann, H., Lehner, I., Seneviratne, S. I., and Wernli, H. (2014). Deuterium excess as a proxy for continental moisture recycling and plant transpiration. *Atmos. Chem. Phys.*, 14 (8):4029–4054. doi:10.5194/acp-14-4029-2014.

Aemisegger, F. and Sjolte, J. (2018). A climatology of strong large-scale ocean evaporation events. Part II: relevance for the deuterium excess signature of the evaporation flux. *J. Climate*, 31:7313–7336. doi:10.1175/JCLI-D-17-0592.1.

Aemisegger, F., Spiegel, J. K., Pfahl, S., Sodemann, H., Eugster, W., and Wernli, H. (2015). Isotope meteorology of cold front passages: a case study combining observations and modeling. *Geophys. Res. Lett.*, 42:5652–5660. doi:10.1002/1099-1085(20000615)14:8<1341::AID-HYP983>3.0.CO;2-Z C.

Aemisegger, F., Vogel, R., Graf, P., Dahinden, F., Villiger, L., Jansen, F., Bony, S., Stevens, B., and Wernli, H. (2020). How Rossby wave breaking modulates the water cycle in the North Atlantic trade wind region. *WCD*, 2020:1–47. doi:10.5194/wcd-2020-51.

Blackmon, M. L., Wallace, J. M., Lau, N.-C., and Mullen, S. L. (1977). An observational study of the Northern Hemisphere wintertime circulation. *J. Atmos. Sci.*, 34(7):1040–1053. doi:10.1175/1520-0469(1977)034<1040:AOSOTN>2.0.CO;2.

Butzin, M., Werner, M., Masson-Delmotte, V., Risi, C., Frankenberg, C., Gribanov, K., Jouzel, J., and Zakharov, V. I. (2014). Variations of oxygen-18 in West Siberian precipitation during the last 50 years. *Atmos. Chem. Phys.*, 14(11):5853–5869. doi:10.5194/acp-14-5853-2014.

Chang, E. K., Lee, S., and Swanson, K. L. (2002). Storm track dynamics. *J. Clim.*, 15(16):2163–2183. doi:10.1175/1520-0442(2002)015<02163:STD>2.0.CO;2.

Charney, J. G. (1947). The dynamics of long waves in a baroclinic westerly current. *J. Meteorol.*, 4(5):136–162.

Christner, E., Aemisegger, F., Pfahl, S., Werner, M., Cauquoin, A., Schneider, M., Hase, F., Barthlott, S., and Schädler, G. (2018). The climatological impacts of continental surface evaporation, rainout, and subcloud processes on δD of water vapor and precipitation in Europe. *J. Geophys. Res. Atmos.*, 123(8):4390–4409. doi:10.1002/2017JD027260.

Cohen, J., Screen, J. A., Furtado, J. C., Barlow, M., Whittleston, D., Coumou, D., Francis, J., Dethloff, K., Entekhabi, D., Overland, J., et al. (2014). Recent Arctic amplification and extreme mid-latitude weather. *Nat. Geosci.*, 7(9):627–637. doi:10.1038/ngeo2234.

Copernicus Climate Change Service (C3S) (2017). ERA5: Fifth generation of ECMWF atmospheric reanalyses of the global climate. Copernicus Climate Change Service Climate Data Store (CDS). Date accessed: 01.01.2020. https://cds.climate.copernicus.eu/cdsapp#!/home.

Copernicus Climate Change Service (C3S) (2018). Dry and warm spring and summer. Date accessed: 05.05.2020. https://climate.copernicus.eu/dry-and-warm-spring-and-summer.

Cowtan, K. and Way, R. G. (2014). Coverage bias in the HadCRUT4 temperature series and its impact on recent temperature trends. *Q. J. Roy. Meteor. Soc.*, 140(683):1935–1944. doi:10.1002/qj.2297.

Craig, H. and Gordon, L. (1965). Deuterium and oxygen-18 variations in the ocean and the marine atmosphere. In Tongiorgi, E., editor, *Stable isotopes in oceanographic studies and paleotemperatures*, pages 9–130. Laboratorio di Geologia Nucleare, Pisa.

Descamps, S., Aars, J., Fuglei, E., Kovacs, K. M., Lydersen, C., Pavlova, O., Pedersen, , Ravolainen, V., and Strøm, H. (2017). Climate change impacts on wildlife in a High Arctic archipelago – Svalbard, Norway. *Glob. Change Biol.*, 23(2):490–502. doi:10.1111/gcb.13381.

Ding, Q., Schweiger, A., L'Heureux, M., Battisti, D. S., Po-Chedley, S., Johnson, N. C., Blanchard-Wrigglesworth, E., Harnos, K., Zhang, Q., Eastman, R., et al. (2017). Influence of high-latitude atmospheric circulation changes on summertime Arctic sea ice. *Nat. Clim. Change*, 7(4):289–295. doi:10.1038/nclimate3241.

Doms, G., Förstner, J., Heise, E., Herzog, H., Mironov, D., Raschendorfer, M., Reinhardt, T., Ritter, B., Schrodin, R., Schulz, J.-P., and Vogel, G. (2011). A description of the nonhydrostatic regional COSMO model. Part II: Physical parameterization. *Deutscher Wetterdienst, Offenbach, Germany.*

Dowdeswell, J., Wadhams, P., Dowdeswell, J. A., and Schofield, A. N. (1995). Glaciers in the High Arctic and recent environmental change. *Philos. T. R. Soc. A.*, 352(1699):321–334. doi:10.1098/rsta.1995.0073.

Dütsch, M., Pfahl, S., Meyer, M., and Wernli, H. (2018). Lagrangian process attribution of isotopic variations in near-surface water vapour in a 30-year regional climate simulation over Europe. *Atmos. Chem. Phys.*, 18(3):1653–1669. doi:10.5194/acp-18-1653-2018.

Eady, E. T. (1949). Long waves and cyclone waves. *Tellus*, 1(3):33–52. doi:10.3402/tellusa.v1i3.8507.

Gat, J. (2010). Isotope hydrology: a study of the water cycle. *Springer Ser. Env. Man.*, 6. doi:10.1142/p027.

Grams, C. M., Wernli, H., Böttcher, M., Čampa, J., Corsmeier, U., Jones, S. C., Keller, J. H., Lenz, C.-J., and Wiegand, L. (2011). The key role of diabatic processes in modifying the upper-tropospheric wave guide: a North Atlantic case-study. *Q. J. R. Meteorol. Soc.*, 137(661):2174–2193. doi:10.1002/qj.891.

Hoffmann, L., Günther, G., Li, D., Stein, O., Wu, X., Griessbach, S., Heng, Y., Konopka, P., Müller, R., Vogel, B., and Wright, J. S. (2019). From ERA-Interim to ERA5: the considerable impact of ECMWF's next-generation reanalysis on Lagrangian transport simulations. *Atmos. Chem. Phys.*, 19(5):3097–3124. doi:10.5194/acp-19-3097-2019.

Hoskins, B. J., McIntyre, M. E., and Robertson, A. W. (1985). On the use and significance of isentropic potential vorticity maps. *Q. J. Roy. Meteor. Soc.*, 111(470):877–946. doi:10.1002/qj.49711147002.

Jansing, L. (2019). Marine boundary layer stable water isotope variability in the Southern Ocean: An investigation using the regional COSMOiso model. Master's thesis, ETH Zurich, Institute for Atmospheric and Climate Science (IAC). doi:10.3929/ethz-b-000438068.

Jay, C. V., Fischbach, A. S., and Kochnev, A. A. (2012). Walrus areas of use in the Chukchi Sea during sparse sea ice cover. *Mar. Ecol. Prog. Ser.*, 468:1–13. doi:10.3354/meps10057.

Johnsen, S. J., Dansgaard, W., and White, J. W. C. (1989). The origin of Arctic precipitation under present and glacial conditions. *Tellus*, 41B (4):452–468. doi:10.1111/j.1600-0889.1989.tb00321.x.

Jouzel, J., Merlivat, L., and Lorius, C. (1982). Deuterium excess in an East Antarctic ice core suggests higher relative humidity at the oceanic surface during the last glacial maximum. *Nature*, 299 (5885):688–691. doi:10.1016/j.quascirev.2006.07.015.

Lee, K.-O., Aemisegger, F., Pfahl, S., Flamant, C., Lacour, J.-L., and Chaboureau, J.-P. (2019). Contrasting stable water isotope signals from convective and large-scale precipitation phases of a heavy precipitation event in southern Italy during HyMeX IOP 13: a modelling perspective. *Atmos. Chem. Phys.*, 19(11):7487–7506. doi:10.5194/acp-19-7487-2019.

Lyon, S., Destouni, G., Giesler, R., Humborg, C., Mörth, C.-M., Seibert, J., Karlsson, J., and Troch, P. A. (2009). Estimation of permafrost thawing rates in a Sub-Arctic catchment using recession flow analysis. *Hydrol. Earth Syst. Sc.*, 13(5):595–604. doi:10.5194/hess-13-595-2009.

Madonna, E., Wernli, H., Joos, H., and Martius, O. (2014). Warm conveyor belts in the ERA-Interim dataset (1979–2010). Part I: Climatology and potential vorticity evolution. *Journal of Climate*, 27(1):3–26. doi:10.1175/JCLI-D-12-00720.1.

Martius, O., Schwierz, C., and Davies, H. (2010). Tropopause-level waveguides. *J. Atmos. Sci.*, 67(3):866–879. doi:10.1175/2009JAS2995.1.

Massacand, A. C., Wernli, H., and Davies, H. C. (2001). Influence of upstream diabatic heating upon an Alpine event of heavy precipitation. *Mon. Weather Rev.*, 129(11):2822–2828. doi:10.1175/1520-0493(2001)129<2822:IOUDHU>2.0.CO;2.

Masson-Delmotte, V., Jouzel, J., Landais, A., Stievenard, M., Johnsen, S. J., White, J. W. C., Werner, M., Sveinbjornsdottir, A., and Fuhrer, K. (2005). GRIP deuterium excess reveals rapid and orbital-scale changes in Greenland moisture origin. *Science*, 309 (5731):118–121. doi:10.1126/science.1108575.

Our Planet (2019). Silverback Films, Netflix, produced by Sophie Lanfear, directed by Alastair Fothergill.

Overpeck, J., Hughen, K., Hardy, D., Bradley, R., Case, R., Douglas, M., Finney, B., Gajewski, K., Jacoby, G., Jennings, A., Lamoureux, S., Lasca, A., MacDonald, G., Moore, J., Retelle, M., Smith, S., Wolfe, A., and Zielinski, G. (1997). Arctic environmental change of the last four centuries. *Science*, 278(5341):1251–1256. doi: 10.1126/science.278.5341.1251.

Pfahl, S., Schwierz, C., Croci-Maspoli, M., Grams, C. M., and Wernli, H. (2015). Importance of latent heat release in ascending air streams for atmospheric blocking. *Nat. Geosci.*, 8(8):610–614.

Pfahl, S. and Wernli, H. (2008). Air parcel trajectory analysis of stable isotopes in water vapor in the eastern Mediterranean. *J. Geophys. Res.*, 113 (D20):D20 104. doi:10.1029/2008JD009839.

Pfahl, S. and Wernli, H. (2012). Quantifying the relevance of atmospheric blocking for co-located temperature extremes in the Northern Hemisphere on (sub-) daily time scales. *Geophys. Res. Lett.*, 39(12). doi:10.1029/2012GL052261.

Pfahl, S., Wernli, H., and Yoshimura, K. (2012). The isotopic composition of precipitation from a winter storm - a case study with the limited-area model $COSMO_{iso}$. *Atmos. Chem. Phys.*, 12(3):1629–1648. doi:10.5194/acp-12-1629-2012.

Schneider, A., Borsdorff, T., aan de Brugh, J., Aemisegger, F., Feist, D. G., Kivi, R., Hase, F., Schneider, M., and Landgraf, J. (2020). First data set of H_2O/HDO columns from the Tropospheric Monitoring Instrument (TROPOMI). *Atmos. Meas. Tech.*, 13(1):85–100. doi:10.5194/amt-13-85-2020.

Schneider et al., A. (in prep. for 2021). Retrieving H_2O/HDO columns over cloudy and clear-sky scenes from the Tropospheric Monitoring Instrument (TROPOMI). *Atmos. Meas. Tech.*

Screen, J. A. and Simmonds, I. (2010). The central role of diminishing sea ice in recent Arctic temperature amplification. *Nature*, 464(7293):1334–1337. doi:10.1038/nature09051.

Serreze, M., Barrett, A., Stroeve, J., Kindig, D., and Holland, M. (2008). The emergence of surface-based Arctic amplification. *The Cryosphere*, 2(4):601–622. doi:10.5194/tc-3-11-2009.

Sinclair, V. A., Mikkola, J., Rantanen, M., and Räisänen, J. (2019). The summer 2018 heatwave in Finland. *Q. J. Roy. Meteor. Soc.*, 74(11):403–409. doi:10.1002/wea.3525.

Sodemann, H., Schwierz, C., and Wernli, H. (2008). Interannual variability of Greenland winter precipitation sources: Lagrangian moisture diagnostic and North Atlantic Oscillation influence. *J. Geophys. Res.*, 113:D03–107. doi:10.1029/2007JD008503.

Sprenger, M., Fragkoulidis, G., Binder, H., Croci-Maspoli, M., Graf, P., Grams, C. M., Knippertz, P., Madonna, E., Schemm, S., Škerlak, B., and Wernli, H. (2017). Global climatologies of Eulerian and Lagrangian flow features based on ERA-Interim reanalyses. *Bull. Amer. Meteor. Soc.*, 98:1739–1748. doi:10.1175/BAMS-D-15-00299.1.

Sprenger, M. and Wernli, H. (2015). The LAGRANTO Lagrangian analysis tool – version 2.0. *Geosci. Model Dev.*, 8 (8):2569–2586. doi:10.5194/gmd-8-2569-2015.

Steffensen, J. P., Andersen, K. K., Bigler, M., Clausen, H. B., Dahl-Jensen, D., Fischer, H., Goto-Azuma, K., Hansson, M., Johnsen, S. J., Jouzel, J., Masson-Delmotte, V., Popp, T., Rasmussen, S. O., Röthlisberger, R., Ruth, U., Stauffer, B., Siggard-Andersen, M.-L., Sveinbjörnsdottir, A. E., Svensson, A., and White, J. W. C. (2008). High-resolution Greenland ice core data show abrupt climate change happens in few years. *Science*, 321 (5889):680–684. doi:10.1126/science.1157707.

Steinfeld, D. (2019). The role of latent heating in atmospheric blocking: climatology and numerical experiments. PhD thesis, ETH Zurich, doi:10.3929/ethz-b-000380041.

Stenni, B., Masson-Delmotte, V., Johnsen, S., Jouzel, J., Longinelli, A., Monnin, E., Röthlisberger, R., and Selmo, E. (2001). An oceanic cold reversal during the last deglaciation. *Science*, 293 (5537):2074–2077. doi:110.1126/science.1059702.

Steppeler, J., Doms, G., Schättler, U., Bitzer, H. W., Gassmann, A., Damrath, U., and Gregoric, G. (2003). Meso-gamma scale forecasts using the nonhydrostatic model LM. *Meteorol. Atmospheric Phys.*, 82(1):75–96. doi:10.1007/s00703-001-0592-9.

Thurnherr, I., Hartmuth, K., Jansing, L., Gehring, J., Boettcher, M., Gorodetskaya, I., Werner, M., Wernli, H., and Aemisegger, F. (2020a). The role of air-sea fluxes for the water vapour isotope signals in the cold and warm sectors of extratropical cyclones over the Southern Ocean. *WCD*, pages 1–42. doi:10.5194/wcd-2020-46.

Thurnherr, I., Kozachek, A., Graf, P., Weng, Y., Bolshiyanov, D., Landwehr, S., Pfahl, S., Schmale, J., Sodemann, H., Steen-Larsen, H. C., Toffoli, A., Wernli, H., and Aemisegger, F. (2020b). Meridional and vertical variations of the water vapour isotopic composition in the marine boundary layer over the Atlantic and Southern Ocean. *Atmos. Chem. Phys.*, 20(9):5811–5835. doi:10.5194/acp-20-5811-2020.

Trigo, R. M., Pozo-Vázquez, D., Osborn, T. J., Castro-Díez, Y., Gámiz-Fortis, S., and Esteban-Parra, M. J. (2004). North Atlantic oscillation influence on precipitation, river flow and water resources in the Iberian Peninsula. *Int. J. Climatol.*, 24(8):925–944. doi:10.1002/joc.1048.

Veefkind, J., Aben, I., McMullan, K., Förster, H., de Vries, J., Otter, G., Claas, J., Eskes, H., de Haan, J., Kleipool, Q., van Weele, M., Hasekamp, O., Hoogeveen, R., Landgraf, J., Snel, R., Tol, P., Ingmann, P., Voors, R., Kruizinga, B., Vink, R., Visser, H., and Levelt, P. (2012). TROPOMI on the ESA Sentinel-5 Precursor: A GMES mission for global observations of the atmospheric composition for climate, air quality and ozone layer applications. *Remote Sens. Environ.*, 120:70 – 83. doi:10.1016/j.rse.2011.09.027.

Vergara-Temprado, J., Ban, N., Panosetti, D., Schlemmer, L., and Schär, C. (2020). Climate models permit convection at much coarser resolutions than previously considered. *J. Clim.*, 33(5):1915–1933. doi:10.1175/JCLI-D-19-0286.1.

Vimeux, F., Masson, V., Jouzel, J., Stievenard, M., and Petit, J. R. (1999). Glacial–interglacial changes in ocean surface conditions in the Southern Hemisphere. *Nature*, 398 (6726):410–413. doi:10.1038/18860.

Watts, J. (2018). The Swedish town on the frontline of the Arctic wildfires. Date accessed: 05.05.2020. https://www.theguardian.com/world/2018/jul/30/the-swedish-town-on-the-frontline-of-the-arctic-wildfires.

Werner, M., Langebroek, P. M., Carlsen, T., Herold, M., and Lohmann, G. (2011). Stable water isotopes in the ECHAM5 general circulation model: Toward high-resolution isotope modeling on a global scale. *J. Geophys. Res. Atmos.*, 116(D15). doi:10.1029/2011JD015681.

Wernli, H. and Davies, H. C. (1997). A Lagrangian-based analysis of extratropical cyclones. I: The method and some applications. *Q.J.R. Meteorol. Soc.*, 123 (538):467–489. doi:10.1002/qj.49712353811.

Wernli, H. and Papritz, L. (2018). Role of polar anticyclones and mid-latitude cyclones for Arctic summertime sea-ice melting. *Nat. Geosci.*, 11(2):108–113. doi:10.1038/s41561-017-0041-0.

Wernli, H. and Schwierz, C. (2006). Surface cyclones in the ERA-40 dataset (1958–2001). Part I: Novel identification method and global climatology. *J. Atmos. Sci.*, 63 (10):2486–2507. doi:10.1175/JAS3766.1.